Effect of gravity on the dynamics of non-isothermic ultra-thin two-layer films

ALEXANDER NEPOMNYASHCHY[1,2] AND ILYA SIMANOVSKII[1]†

[1]Department of Mathematics, Technion – Israel Institute
of Technology, 32000 Haifa, Israel

[2]Minerva Center for Nonlinear Physics of Complex Systems, Technion – Israel Institute
of Technology, 32000 Haifa, Israel

The effect of gravity on the dynamics of non-isothermic ultra-thin two-layer films is studied in this paper. The joint action of disjoining pressure and thermocapillary forces is taken into account. The problem is considered in a long-wave approximation. The linear stability of a quiescent state and thermocapillary flows is investigated. It has been found that the influence of the upper fluid density is significantly stronger than that of the difference of fluid densities. Nonlinear flow regimes are studied by means of numerical simulations. The gravity can lead to the formation of stripes or holes instead of droplets. The two-dimensional wavy patterns are replaced by one-dimensional waves with the fronts inclined or transverse to the direction of the horizontal temperature gradient.

Key words: instability, lubrication theory

1. Introduction

In the last few decades, the development of microfluidics and nanotechnology has led to a significant progress in the exploration of thin film flows. When the layers are sufficiently thin, the flows are strongly affected by interfacial phenomena, specifically by the Marangoni effect. The Marangoni convection in layered fluid systems has been studied in the case of a temperature gradient applied across the layers and in the case of a temperature gradient directed along the interfaces, as well as for a temperature gradient inclined with respect to the interface (Davis 1987; Simanovskii & Nepomnyashchy 1993; Nepomnyashchy, Simanovskii & Legros 2006). The Marangoni effect strongly influences the stability of flowing films (Miladinova *et al.* 2002*a,b*; Demekhin, Kalliadasis & Velarde 2006; Trevelyan *et al.* 2007).

The dynamics of ultra-thin (but still macroscopic) films, with the thickness less than 100 nm, is of a special interest. Such kind of flows has numerous technological applications (coating, flotation, biological membranes, adhesives, etc.). The instabilities in thin films are of potential use in the formation of regular nanostructures and ordered porous membranes, in soft lithographic techniques and in other areas of nanotechnology. For the description of the ultra-thin film dynamics, it is necessary to take into account the long-range intermolecular forces (first of all, van der Waals forces), acting between molecules of the liquid and substrate (Israelachvili 1992).

† Email address for correspondence: yuri11@inter.net.il

It is essential that these forces act on distances that are large relative to interatomic distances. Hence, despite their microscopic origin, they can be incorporated into a macroscopic theory.

In the framework of the continuum approach, the van der Waals forces manifest themselves in the disjoining pressure (Williams & Davis 1982; Sharma & Ruckenstein 1986), which can be derived from the potential energy of intermolecular interactions. Hydrodynamic behaviour of thin films has been extensively studied (see Oron, Davis & Bankoff 1997 and Sharma 2003 for review). A destabilizing disjoining pressure may lead to a true rupture of the film. Otherwise, the development of instability is similar to a phase separation when the unstable 'phase' with an intermediate value of h is destroyed, and the system is separated into two stable 'phases': a thin film and a thick film (Sharma 2003; Thiele 2003).

In some coating processes and biological systems, liquid films can be composed of several liquid layers. Specifically, a lower film obtained by a liquid coating of a substrate can be used in order to significantly change the stability properties of the upper film. A two-layer liquid system driven by Marangoni stresses and influenced by van der Waals forces has been considered by Craster & Matar (2000) and Matar, Craster & Warner (2002) by modelling a liquid lung lining. An example of a biological three-layer systems is a tear film, which consists of an aqueous layer sandwiched between a mucous layer and a lipid layer; its break-up is induced by long-range intermolecular forces (Sharma, Khanna & Reiter 1999). Recently, a series of experiments have been carried out on the stability of systems which consist of two immiscible thin films on a solid substrate (Higgins & Jones 2000; Lin *et al.* 2001, 2002*a,b*).

Dynamics of multilayer ultra-thin films are characterized by several Hamaker constants, which can be of different signs; therefore, they can be much richer. A theoretical description of two-layer ultra-thin films has been developed by Pototsky *et al.* (2004, 2005, 2006), Bandyopadhyay, Gulabani & Sharma (2005), Fisher & Golovin (2005) and Bandyopadhyay & Sharma (2006).

The dynamics of ultra-thin films under the joint action of the Marangoni effect and the van der Waals forces have not yet been explored extensively. The authors are not aware of any experimental works on that subject. There is a number of theoretical papers where instabilities of ultra-thin films have been considered. A general structure of the evolution equations has been studied by Merkt *et al.* (2005) and Pototsky *et al.* (2005). The development of instabilities has been studied in the case of a temperature gradient directed along the interfaces (Nepomnyashchy & Simanovskii 2006) and across the layers (Joo & Hsieh 2000; Nepomnyashchy & Simanovskii 2007), as well as in the case where the temperature gradient is inclined with respect to the interfaces (Nepomnyashchy & Simanovskii 2009*a,b*). It has been found that for sufficiently large values of the ratio between the longitudinal and transverse Marangoni numbers, the real part of the linear growth rate does not depend on the direction of the wavenumber, except the case of nearly longitudinal disturbances. Numerous types of nonlinear evolution have been observed, which include ordered systems of droplets, 'splashes', oblique waves, modulated transverse and longitudinal structures.

As a rule, the influence of the gravity on the ultra-thin film dynamics is neglected. Indeed, the disjoining pressure varies with the film thickness h as $1/h^3$, while the hydrostatic pressure is proportional to h. Therefore, the ratio of the hydrostatic pressure to the disjoining pressure decreases as h^4. Surprisingly, the effect of gravity on the film stability can be significant. As has been shown for an isothermal two-layer film by Fisher & Golovin (2005), the hydrostatic pressure cannot be neglected in
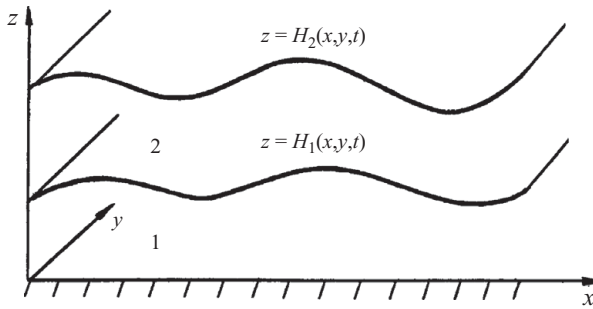
FIGURE 1. Geometric configuration of the region and coordinate axes.

the case where the Hamaker constants are of different signs and can 'cancel each other'. While the linear stability threshold is weakly affected by gravity, the nonlinear development of instability is rather sensitive to the influence of the hydrostatic pressure. Specifically, decomposition of the film into droplets can be replaced by the appearance of holes. Besides, a flattening of the droplet shapes is observed.

In this paper, we consider the influence of the gravity on the instabilities of non-isothermic two-layer films. The mathematical model is formulated in §2. In §3, we develop the linear stability theory. The nonlinear dynamic regimes are described in §4. Section 5 contains concluding remarks.

2. Long-wave evolution equations

2.1. *Formulation of the problem*

Consider a system of two superposed layers of immiscible liquids with different physical properties (see figure 1). The bottom layer rests on a solid substrate and the top layer is in contact with the adjacent gas phase. The temperature of the solid substrate is $T_s + Ax$ and the temperature of the gas is $T_g + Ax$. All the variables referring to the bottom layer are marked by subscript 1 and all the variables referring to the top layer are marked by subscript 2. The coordinates of the interfaces in a quiescent state are H_i^0, $i = 1, 2$. The deformable interfaces are described by equations $z = H_1(x, y, t)$ (liquid–liquid interface) and $z = H_2(x, y, t)$ (liquid–gas interface). The ith fluid has density ρ_i, kinematic viscosity ν_i, dynamic viscosity $\eta_i = \rho_i \nu_i$, thermal diffusivity χ_i and heat conductivity κ_i. The surface tension coefficients on the lower and upper interfaces, σ_1 and σ_2, are linear functions of temperature T: $\sigma_1 = \sigma_1^0 - \alpha_1 T$ and $\sigma_2 = \sigma_2^0 - \alpha_2 T$. The gravity acceleration is g.

In the case of thin-film flows, when the fluid system is thin in one direction and extended in other directions, the nonlinear model governing three-dimensional flows with a deformable interface can be drastically simplified by means of a long-wavelength expansion. The leading order of this expansion is known as the 'lubrication approximation'. The long-wave approach is based on the assumption that the characteristic spatial scales in the x- and y-directions are much larger than that in the z-direction. It is assumed that the solution of the problem depends on the scaled horizontal coordinates, $X = \epsilon x$ and $Y = \epsilon y$, $\epsilon \ll 1$, rather than on x and y. Also, it is assumed that the solution depends on the scaled time variable $\tau = \epsilon t$. The details of the long-wave approach can be found in review papers (Davis 1987; Oron *et al.* 1997).

2.2. *Thermocapillary flows*

First, let us derive the long-wave evolution equations for a thermocapillary flow, neglecting the interfacial tensions and the van der Waals forces.

To the leading order, the evolution of the system is governed by the following equations and boundary conditions:

$$U_{1zz} = 0, \ V_{1zz} = 0, \ U_{1X} + V_{1Y} + W_{1z} = 0, \ T_{1zz} = 0, \ 0 < z < H_1, \qquad (2.1)$$

$$U_{2zz} = 0, \ V_{2zz} = 0, \ U_{2X} + V_{2Y} + W_{2z} = 0, \ T_{2zz} = 0, \ H_1 < z < H_2, \qquad (2.2)$$

$$z = 0 : \ U_1 = V_1 = W_1 = 0, \ T_1 = T_s + Ax, \qquad (2.3)$$

$$z = H_1 : \ U_1 = U_2, \ V_1 = V_2, \ W_1 = W_2, \qquad (2.4)$$

$$\eta_2 U_{2z} - \eta_1 U_{1z} - \alpha_1 (T_{1X} + H_{1X} T_{1z}) = 0, \qquad (2.5)$$

$$\eta_2 V_{2z} - \eta_1 V_{1z} - \alpha_1 (T_{1Y} + H_{1Y} T_{1z}) = 0, \qquad (2.6)$$

$$H_{1\tau} + U_1 H_{1X} + V_1 H_{1Y} = W_1, \qquad (2.7)$$

$$T_1 = T_2, \ \kappa_1 T_{1z} = \kappa_2 T_{2z}, \qquad (2.8)$$

$$z = H_2 : \ -\eta_2 U_{2z} - \alpha_2 (T_{2X} + H_{2X} T_2) = 0, \qquad (2.9)$$

$$-\eta_2 V_{2z} - \alpha_2 (T_{2Y} + H_{2Y} T_{2z}) = 0, \qquad (2.10)$$

$$H_{2\tau} + U_2 H_{2X} + V_2 H_{2Y} = W_2, \qquad (2.11)$$

$$\kappa_2 T_{2z} = -q(T_2 - T_g - Ax), \qquad (2.12)$$

where subscripts z, X, Y and τ denote corresponding partial derivatives, and U_j, V_j and W_j, $j = 1, 2$, are the leading-order terms in the expansions of velocity coordinates in powers of ϵ:

$$u_{xj} = U_j + \cdots, \ u_{yj} = V_j + \cdots, \ u_{zj} = \epsilon W_j + \cdots. \qquad (2.13)$$

The variable q is the heat exchange coefficient which is assumed to be constant. Solving the problem for the temperature fields, we find that

$$T_1 = T_s - (T_s - T_g) D q \kappa_2 z + Ax, \qquad (2.14)$$

$$T_2 = T_s - (T_s - T_g) D q [(\kappa_2 - \kappa_1) H_1 + \kappa_1 z] + Ax, \qquad (2.15)$$

where

$$D = [\kappa_1 \kappa_2 + q(\kappa_2 - \kappa_1) H_1 + q \kappa_1 H_2]^{-1}. \qquad (2.16)$$

The x-components of the flow velocities generated by the thermocapillary stresses are determined by the following formulae:

$$U_1 = \frac{(T_s - T_g)\kappa_2}{\eta_1} [D(\alpha_1 q H_1 - \alpha_2 \kappa_1)]_X z - \frac{(\alpha_1 + \alpha_2)A}{\eta_1} z, \qquad (2.17)$$

$$U_2 = \frac{(T_s - T_g)\kappa_2}{\eta_2} \left\{ -\alpha_2 \kappa_2 D_X z + \frac{H}{\eta_1} [D(\alpha_1 \eta_2 q H_1 - \alpha_2 (\eta_2 - \eta_1) \kappa_1)_X]_X \right\}$$
$$- \left[\frac{\alpha_2}{\eta_2}(z - H_1) + \frac{\alpha_1 + \alpha_2}{\eta_1} H_1 \right] A. \qquad (2.18)$$

The expressions for y-components of the flow velocities, V_1 and V_2, can be obtained from U_1 and U_2 by replacing X by Y. Solving the continuity equations with respect to W_1 and W_2 with corresponding boundary conditions, we find that

$$W_1(X, Y, H_1) = -\int_0^{H_1} (U_{1X} + V_{1Y}) \, dz, \tag{2.19}$$

$$W_2(X, Y, H_2) = -\int_0^{H_1} (U_{1X} + V_{1Y}) \, dz + \int_{H_1}^{H_2} (U_{2X} + V_{2Y}) \, dz. \tag{2.20}$$

Using (2.19) and (2.20), we rewrite the kinematic conditions (2.7) and (2.11) in the following form:

$$H_{1\tau} + \left(\int_0^{H_1} U_1 \, dz \right)_X + \left(\int_0^{H_1} V_1 \, dz \right)_Y = 0, \tag{2.21}$$

$$H_{2\tau} + \left(\int_0^{H_1} U_1 \, dz + \int_{H_1}^{H_2} U_2 \, dz \right)_X + \left(\int_0^{H_1} V_1 \, dz + \int_{H_1}^{H_2} V_2 \, dz \right)_Y = 0. \tag{2.22}$$

Substituting expressions for flow velocities obtained above into (2.21) and (2.22), we arrive at a closed system of equations that govern the evolution of a heated two-layer film under the action of the thermocapillary effect:

$$H_{1\tau} + \nabla \cdot \boldsymbol{Q}_1^T = 0, \quad H_{2\tau} + \nabla \cdot \boldsymbol{Q}_2^T = 0, \tag{2.23}$$

where

$$\boldsymbol{Q}_1^T = \frac{(T_s - T_g)\kappa_2}{2\eta_1} H_1^2 \nabla [D(q\alpha_1 H_1 - \alpha_2 \kappa_1)] - \frac{(\alpha_1 + \alpha_2)A}{2\eta_1} H_1^2 \boldsymbol{e}_x, \tag{2.24}$$

$$\boldsymbol{Q}_2^T = \frac{(T_s - T_g)}{2\eta_1 \eta_2} \left\{ H_2^2 \nabla [(-\alpha_2 \kappa_1 \eta_1)D] + (2H_2 - H_1)H_1 \nabla \{ D[q\alpha_1 \eta_2 H_1 \right.$$
$$\left. - \alpha_2 \kappa_1 (\eta_2 - \eta_1)] \} \right\} - \left[\frac{\alpha_2 A}{2\eta_2} (H_2 - H_1)^2 + \frac{\alpha_1 + \alpha_2}{2\eta_1} A H_1 (2H_2 - H_1) \right] \boldsymbol{e}_x, \tag{2.25}$$

where $\boldsymbol{e}_x$ is the unit vector of the axis x.

2.3. *Flows in the presence of interfacial tensions and van der Waals forces*

In the framework of the continuum approach, the van der Waals forces manifest themselves as external normal stresses ('disjoining pressures') imposed on each interface (Israelachvili 1992). The disjoining pressures modify the dependences of the pressures P_1 and P_2 in each layer on the layers' thicknesses H_1 and H_2 as follows (Fisher & Golovin 2005):

$$P_1 = -\sigma_1 \nabla^2 H_1 - \sigma_2 \nabla^2 H_2 + W_1(H_1, H_2), \tag{2.26}$$

$$P_2 = -\sigma_2 \nabla^2 H_2 + W_2(H_1, H_2), \tag{2.27}$$

where

$$W_1(H_1, H_2) = \frac{A_{sg} - A_{s2} - A_{g1}}{6\pi H_2^3} + \frac{A_{s2}}{6\pi H_1^3} + \rho_1 g H_1 + \rho_2 g (H_2 - H_1), \tag{2.28}$$

$$W_2(H_1, H_2) = \frac{A_{sg} - A_{s2} - A_{g1}}{6\pi H_2^3} + \frac{A_{g1}}{6\pi (H_2 - H_1)^3} + \rho_2 g H_2. \tag{2.29}$$

Here A_{sg}, A_{s2} and A_{g1} are Hamaker constants, characterizing the interactions between the solid substrate and the gas across the two layers, between the solid substrate and

an infinite layer of liquid 2 across liquid 1, and between the gas phase and an infinite layer of liquid 1 across liquid 2, respectively (see Fisher & Golovin 2005).

Recall that in the case of a one-layer film, the influence of the intermolecular forces is determined by a single Hamaker constant, and the dependence of the interaction energy between the gas phase and the substrate on the thickness of the layer is monotonic. Depending on the sign of the Hamaker constant, the film is either stable or unstable. In the unstable case, the development of the van der Waals instability leads to the film rupture, if it is not stopped by a repulsive interaction of another physical nature (e.g. by electrostatic interaction or steric repulsion).

As we have seen, in the case of a two-layer film the problem is characterized by three non-dimensional Hamaker constants: A_{sg}, A_{s2} and A_{g1}. The Hamaker constants are determined by the dielectric permittivities of all the media as functions of the frequency (Lifshitz & Pitaevskii 1980; Israelachvili 1992), and they mainly depend on the zero-frequency dielectric constants and high-frequency refractive indices of the media (Israelachvili 1992; Pototsky et al. 2005). The signs of Hamaker constants can be different.

If $A_{s2} > 0$ or $A_{g1} > 0$, the effective interactions between corresponding adjacent interfaces are attractive, and they lead to a rupture of the bottom or top layer, respectively. A more interesting situation takes place when $A_{s2} < 0$ and $A_{g1} < 0$, but $A_{sg} - A_{s2} - A_{g1} > 0$, i.e. the effective interaction between the liquid 2/gas interface and the liquid 1/substrate interface is attractive, while the effective interaction between adjacent interfaces is repulsive, one can expect that a van der Waals instability will develop, but it will not lead to the rupture of the layers (Fisher & Golovin 2005). Instead of rupture, one will observe a certain kind of 'spinodal decomposition' of the film into localized 'droplets' and a thin 'precursor' film (Fisher & Golovin 2005; Nepomnyashchy & Simanovskii 2006). Hence, a continuum mechanics approach is valid. In the present paper, we consider solely the case where $A_{sg} - A_{s2} - A_{g1} > 0$, $A_{s2} < 0$ and $A_{g1} < 0$.

In the framework of the lubrication approximation, we arrive at the following evolution equations, which are valid in the case of an inclined temperature gradient:

$$H_{1\tau} + \nabla \cdot \left(\boldsymbol{Q}_1^T + \boldsymbol{Q}_1^{vdW} \right) = 0, \quad H_{2\tau} + \nabla \cdot \left(\boldsymbol{Q}_2^T + \boldsymbol{Q}_2^{vdW} \right) = 0, \tag{2.30}$$

where

$$\boldsymbol{Q}_1^{vdW} = F_{11} \nabla P_1 + F_{12} \nabla P_2, \quad \boldsymbol{Q}_2^{vdW} = F_{21} \nabla P_1 + F_{22} \nabla P_2, \tag{2.31}$$

where $\boldsymbol{Q}_1^T$ and $\boldsymbol{Q}_2^T$ are determined by (2.24) and (2.25).

The pressures P_1 and P_2 are determined by expressions (2.26) and (2.27), and following are the mobility functions:

$$\left. \begin{array}{l} F_{11} = -\dfrac{1}{3\eta_1} H_1^3, \; F_{12} = -\dfrac{1}{2\eta_1} H_1^2 (H_2 - H_1), \; F_{21} = \dfrac{1}{6\eta_1} H_1^3 - \dfrac{1}{2\eta_1} H_1^2 H_2, \\[2mm] F_{22} = (H_2 - H_1) \left[H_1^2 \left(\dfrac{1}{2\eta_1} - \dfrac{1}{3\eta_2} \right) + H_1 H_2 \left(-\dfrac{1}{\eta_1} + \dfrac{2}{3\eta_2} \right) - \dfrac{1}{3\eta_2} H_2^2 \right]. \end{array} \right\} \tag{2.32}$$

Let us transform (2.30) to a non-dimensional form. The natural vertical length scale is the initial thickness of the lower layer, H_1^0. In Fisher & Golovin (2005), the horizontal length scale,

$$L^* = \left(H_1^0 \right)^2 \sqrt{6\pi \sigma_1^0 / |A_{sg}|}, \tag{2.33}$$

has been suggested, which is convenient for the analysis of the instability induced by intermolecular forces. We choose

$$\tau^* = \frac{\eta_1 (L^*)^4}{\sigma_1^0 (H_1^0)^3} \tag{2.34}$$

as a time scale and

$$p^* = \frac{\sigma_1^0 H_1^0}{(L^*)^2} \tag{2.35}$$

as a pressure scale.

Equations (2.30), when written in the non-dimensional form, look as follows:

$$h_{1\tau} + \nabla \cdot \boldsymbol{q}_1 = 0, \quad h_{2\tau} + \nabla \cdot \boldsymbol{q}_2 = 0, \tag{2.36}$$

$$\boldsymbol{q}_1 = f_{11} \nabla p_1 + f_{12} \nabla p_2 + \boldsymbol{q}_1^T, \quad \boldsymbol{q}_2 = f_{21} \nabla p_1 + f_{22} \nabla p_2 + \boldsymbol{q}_2^T, \tag{2.37}$$

where $h_j = H_j / H_1^0$, $p_j = P_j / p^*$, $j = 1, 2$,

$$f_{11} = -\tfrac{1}{3} h_1^3, \quad f_{12} = -\tfrac{1}{2} h_1^2 (h_2 - h_1), \tag{2.38}$$

$$f_{21} = \frac{1}{6} h_1^3 - \frac{1}{2} h_1^2 h_2, \quad f_{22} = (h_2 - h_1) \left[h_1^2 \left(\frac{1}{2} - \frac{\eta}{3} \right) + h_1 h_2 \left(-1 + \frac{2\eta}{3} \right) - \frac{\eta}{3} h_2^2 \right]. \tag{2.39}$$

We use the same notation, τ and ∇, for new, non-dimensional variables. Later on, we assume that the dependence of interfacial tensions on the temperature is relatively weak and can be neglected in the boundary conditions for normal stresses (but not in those for tangential stresses where it is the source of a thermocapillary motion). The contributions of disjoining pressures and hydrostatic pressures are included:

$$p_1 = -\nabla^2 h_1 - \sigma \nabla^2 h_2 + w_1(h_1, h_2), \tag{2.40}$$

$$p_2 = -\sigma \nabla^2 h_2 + w_2(h_1, h_2), \tag{2.41}$$

$$w_1 = \frac{a_0 - a_1 - a_2}{h_2^3} + \frac{a_1}{h_1^3} + g_1 h_1 + g_2 (h_2 - h_1), \tag{2.42}$$

$$w_2 = \frac{a_0 - a_1 - a_2}{h_2^3} + \frac{a_2}{(h_2 - h_1)^3} + g_2 h_2. \tag{2.43}$$

The non-dimensional expressions for the fluxes generated by the thermocapillary effect are the following:

$$\boldsymbol{q}_1^T = \frac{M_\perp}{2} h_1^2 \nabla [d(Bi\, h_1 - \alpha \kappa)] - \frac{M_\parallel}{2} (1 + \alpha) h_1^2 \boldsymbol{e}_x, \tag{2.44}$$

$$\boldsymbol{q}_2^T = \frac{M_\perp}{2} \left\{ -h_2^2 \nabla (d\eta \alpha \kappa) + (2h_2 - h_1) h_1 \nabla \{ d[Bi\, h_1 - \alpha \kappa (1 - \eta)] \} \right\}$$
$$- \frac{M_\parallel}{2} \left[\eta \alpha h_2^2 + (1 + \alpha - \eta \alpha) h_1 (2h_2 - h_1) \right] \boldsymbol{e}_x. \tag{2.45}$$

Here

$$M_\perp = \frac{\alpha_1 (T_s - T_g)}{\sigma_1^0} \left(\frac{L^*}{H_1^0} \right)^2, \tag{2.46}$$

$$M_\parallel = \frac{\alpha_1 A L^*}{\sigma_1^0} \left(\frac{L^*}{H_1^0} \right)^2 \tag{2.47}$$

are the modified transverse and longitudinal Marangoni numbers, respectively,

$$Bi = \frac{q H_1^0}{\kappa_2} \tag{2.48}$$

is the Biot number,

$$d = [\kappa + Bi(1 - \kappa)h_1 + Bi\kappa h_2]^{-1}, \tag{2.49}$$

$\eta = \eta_1/\eta_2$, $\kappa = \kappa_1/\kappa_2$, $\sigma = \sigma_2^0/\sigma_1^0$, $\alpha = \alpha_2/\alpha_1$,

$$a_0 = \text{sign}(A_{sg}), \ a_1 = \frac{A_{s2}}{|A_{sg}|}, \ a_2 = \frac{A_{g1}}{|A_{sg}|}, \tag{2.50}$$

$$g_{1,2} = 6\pi\rho_{1,2}g\left(H_1^0\right)^4/|A_{sg}|. \tag{2.51}$$

If the scaling of the horizontal length is chosen as (2.33), then $|a_0| = 1$.

The system of equations (2.36) contains 12 non-dimensional parameters: $M_\perp$, $M_\parallel$, Bi, σ, α, η, κ, g_1, g_2, a_0, a_1 and a_2.

Let us estimate the characteristic values of these parameters. Fisher & Golovin (2005) showed that for $H_1^0 \sim 100$ nm, the typical values of parameter L^* determined by (2.33) are between 20 and 200 μm. Thus, the ratio $\epsilon = H_1^0/L^*$ is between 5×10^{-4} and 5×10^{-3}, which justifies the long-wave approach. The characteristic values of g_1 and g_2 are between 2×10^{-4} and 2×10^{-2}. The Marangoni numbers are determined by the intensity of the external heating. The assumption that the surface-tension coefficients are linear functions of the temperature is reasonable when $\alpha_j|T_s - T_g| \ll \sigma_j^0$ and $\alpha_j A L \ll \sigma_j^0$, $j = 1, 2$, where L is the characteristic size of the system in the x-direction. Therefore, the modified Marangoni numbers should satisfy the conditions $M_\perp \ll \epsilon^{-2}$ and $M_\parallel \ll \epsilon^{-2}(L^*/L)$. The Biot number characterizes the heat transfer at the free boundary. Generally, one can expect that this parameter is rather small in the case of a thin layer. However, the evaporation of a film can significantly increase cooling at the liquid/gas interface and hence the effective Biot number (Colinet et al. 2003; Haut & Colinet 2005). Other six parameters are intrinsic characteristics of the multilayer system substrate/liquid 1/liquid 2/gas. Parameters α, η and σ are just ratios of physical parameters of the liquids, while a_0, a_1 and a_2 depend on the values of the Hamaker constants A_{sg}, A_{s2} and A_{g1}.

3. Linear stability theory

As mentioned in §2, we consider the case $a_0 = 1$, $a_1 < 0$ and $a_2 < 0$, where the effective interaction between the outer interfaces of the system is attractive and creates a van der Waals instability, while the interaction between the liquid/liquid interface and the outer interfaces is repulsive. In numerical examples, we fix the following values of parameters: $a_1 = -0.4$, $a_2 = -0.1$, $\eta = 1.2$, $\sigma = 0.8$, $\kappa = 1$, $\alpha = 1$, $h_1 = 1$ and $h_2 = 2.5$.

3.1. Dispersion relation

Let us consider a parallel thermocapillary flow with plane interfaces located at $z = H_1^0$ and $z = H_2^0$. This flow corresponds to the basic solution of (2.36):

$$h_1 = 1, \ h_2 = h = 1 + a, \tag{3.1}$$

where $h = H_2^0/H_1^0$ and $a = (H_2^0 - H_1^0)/H_1^0$.

In order to investigate the stability of the plane two-layer film, we substitute

$$h_1 = 1 + \tilde{h}_1, \ h_2 = 1 + a + \tilde{h}_2 \tag{3.2}$$

into (2.36), and linearize them with respect to variables $\tilde{h}_1$ and $\tilde{h}_2$.

The solutions of the linear problem can be written as

$$\tilde{h}_j(X, Y, \tau) = \bar{h}_j \exp(i\mathbf{k} \cdot \mathbf{R} + \lambda\tau), \quad j = 1, 2, \tag{3.3}$$

where $\mathbf{R} = (X, Y)$, $\mathbf{k} = (k_x, k_y)$ is the wave vector, λ is the growth rate and $\bar{h}_j$, $j = 1, 2$, are constants. Substituting (3.3) into the linearized equations, we obtain a dispersion relation

$$\det(\mathbf{N} - \lambda\mathbf{I}) = 0, \tag{3.4}$$

which determines the eigenvalues $\lambda(\mathbf{k})$. Here $\mathbf{I}$ is the unit matrix, while matrix $\mathbf{N}$ can be presented in the following form:

$$\mathbf{N} = \mathbf{B} + \frac{M_\perp Bik^2\kappa}{2(\kappa + Bi + Bi\kappa a)^2}\mathbf{C} + ik_x M_\parallel \mathbf{D}. \tag{3.5}$$

Matrix $\mathbf{B}$ presents the contribution of the van der Waals forces, gravity and surface tensions, and it has the following components:

$$B_{11} = -\frac{k^2}{3}(k^2 - 3a_1 + g_1 - g_2) - \frac{3k^2 a_2}{2a^3}, \tag{3.6}$$

$$B_{12} = -k^2\left(\frac{1}{3} + \frac{a}{2}\right)\left[\sigma k^2 - \frac{3(a_0 - a_1 - a_2)}{(a+1)^4} + g_2\right] + \frac{3k^2 a_2}{2a^3}, \tag{3.7}$$

$$B_{21} = -k^2\left(\frac{1}{3} + \frac{a}{2}\right)(k^2 - 3a_1 + g_1 - g_2) + \left[\frac{1}{2} - \frac{\eta}{3} + (a+1)\left(-1 + \frac{2\eta}{3}\right)\right.$$
$$\left. -\frac{\eta}{3}(a+1)^2\right]\frac{3k^2 a_2}{a^3}, \tag{3.8}$$

$$B_{22} = -k^2\left(\frac{1}{3} + \frac{a}{2}\right)\left[\sigma k^2 - \frac{3(a_0 - a_1 - a_2)}{(a+1)^4} + g_2\right] + ak^2\left[\frac{1}{2} - \frac{\eta}{3}\right.$$
$$\left. +(a+1)\left(-1 + \frac{2\eta}{3}\right) - \frac{\eta}{3}(a+1)^2\right]\left[\sigma k^2 - \frac{3(a_0 - a_1 - a_2)}{(a+1)^4} - \frac{3a_2}{a^4} + g_2\right]. \tag{3.9}$$

One can see that in the framework of the linear stability theory, the action of the gravity is equivalent to the replacement of the van der Waals coefficients, a_0, a_1 and a_2, by a renormalized coefficients, $\hat{a}_0$, $\hat{a}_1$ and $\hat{a}_2$, determined by the following relations:

$$\hat{a}_1 = a_1 - (g_1 - g_2)/3, \quad \hat{a}_2 = a_2, \tag{3.10}$$

$$\hat{a}_0 - \hat{a}_1 - \hat{a}_2 = a_0 - a_1 - a_2 - g_2(a+1)^4/3. \tag{3.11}$$

Hence, one can see that the van der Waals instability, which is related to the positive value of $a_0 - a_1 - a_2$, is weakened with the growth of the upper liquid density (parameter g_2), while the stabilizing action of the negative parameter a_1 is enhanced in the case of a stable density stratification ($g_1 > g_2$) and diminished by the unstable density stratification ($g_1 < g_2$).

The second and third terms on the right-hand side of (3.5) are caused by the thermocapillary effect. The elements of matrix $\mathbf{C}$ are as follows:

$$C_{11} = 1 + Bi(a+1) + \alpha(1 - \kappa), \tag{3.12}$$

$$C_{12} = \alpha\kappa - Bi, \tag{3.13}$$

$$C_{21} = \eta\alpha a^2(1 - \kappa) + (2a+1)[\alpha(1 - \kappa) + 1 + Bi(a+1)], \tag{3.14}$$

$$C_{22} = \eta\alpha\kappa a^2 + (2a+1)(\alpha\kappa - Bi). \tag{3.15}$$

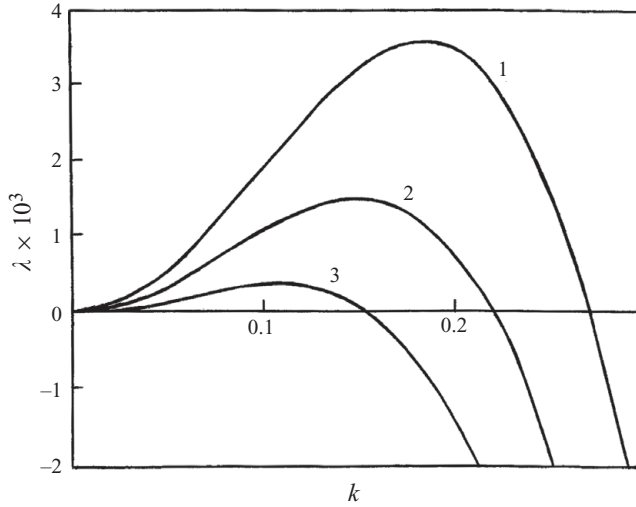FIGURE 2. Dependences of the growth rate λ on the wavenumber k for $g_1 = g_2 = 0$ (line 1), $g_1 = g_2 = 0.02$ (line 2) and $g_1 = g_2 = 0.04$ (line 3).
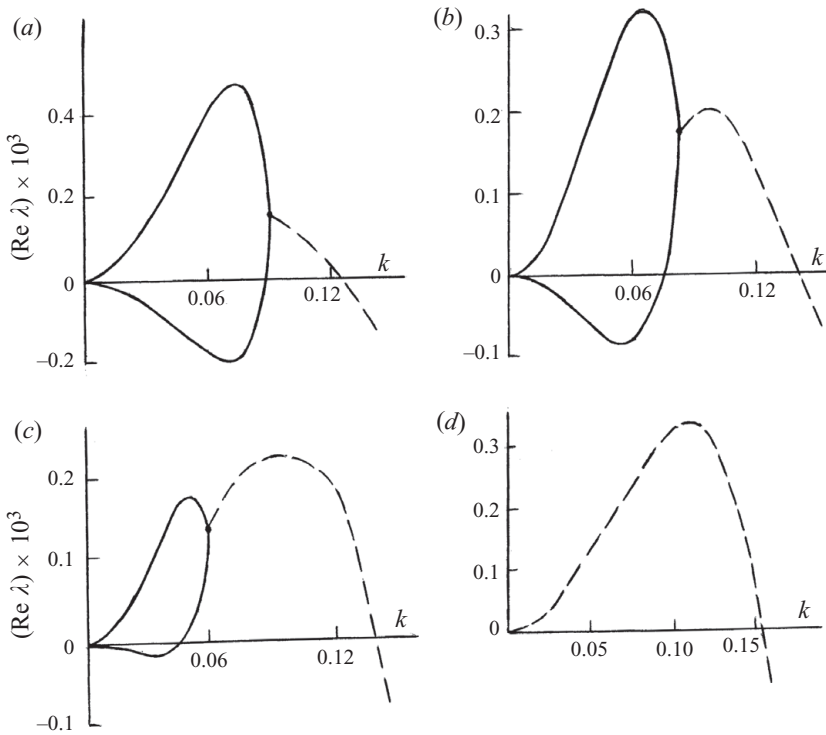

FIGURE 3. Dependences of the growth rate $\mathrm{Re}\,\lambda$ on the wavenumber k for monotonic modes (solid lines) and oscillatory mode (dashed line). (a) $M_\perp = -5$; (b) $M_\perp = -5.2$; (c) $M_\perp = -5.4$; (d) $M_\perp = -5.7$.

The elements of matrix $\boldsymbol{D}$ are as follows:

$$D_{11} = 1 + \alpha, \; D_{12} = 0, \; D_{21} = (a/2)[1 + \alpha(1 - \eta)], \; D_{22} = 1 + \alpha(1 + \eta a). \qquad (3.16)$$
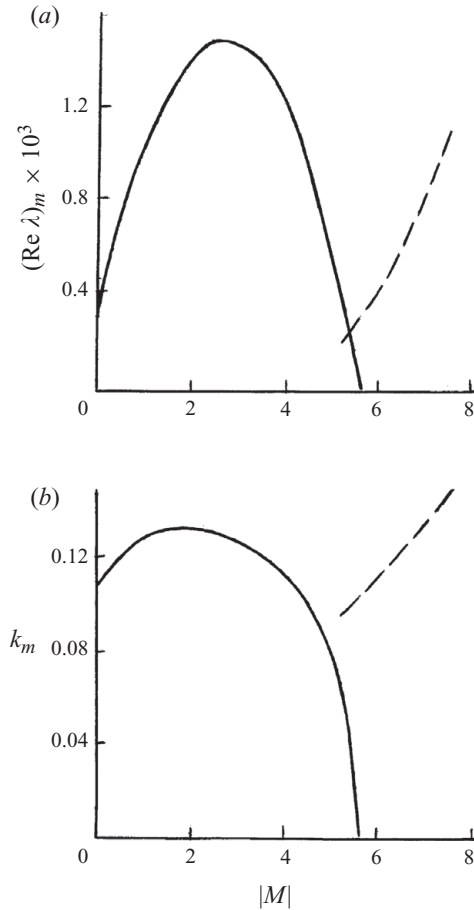
FIGURE 4. Dependences of (*a*) the maximum growth rate $\mathrm{Re}\,\lambda_m$ and (*b*) the corresponding wavenumber k_m on $|M_\perp|$ for the monotonic mode (solid line) and the oscillatory mode (dashed line).

3.2. *Isothermic film*

First, let us discuss the influence of the gravity on the van der Waals instability in the absence of heating ($M_\perp = M_\parallel = 0$).

The major factor is the stabilizing effect of the parameter g_2, which is described by (3.11) (see figure 2). The influence of the density stratification parameter $g_1 - g_2$, described by (3.10), is much weaker. For the values of the parameters corresponding to figure 2, for a fixed value of $g_2 = 0.02$, the derivative $d\lambda_m/dg_1 \approx 7 \times 10^{-4}$ in the interval $0.01 \leqslant g_1 \leqslant 0.03$. (Here $\lambda_m = \max_k \lambda(k)$.)

3.3. *The case of a vertical temperature gradient*

In the presence of a vertical temperature gradient ($M_\parallel = 0$, $M_\perp \neq 0$), an additional instability mechanism appears, which is caused by the Marangoni effect. The interplay of the van der Waals and Marangoni instability mechanisms in the absence of gravity has been studied in detail by Nepomnyashchy & Simanovskii (2007). An example of the transition from the monotonic van der Waals instability to an oscillatory Marangoni instability by heating from above ($M_\perp < 0$) for the values of parameters $g_1 = 0.02$, $g_2 = 0.04$ and $Bi = 10$ is shown in figure 3. The oscillatory instability mode
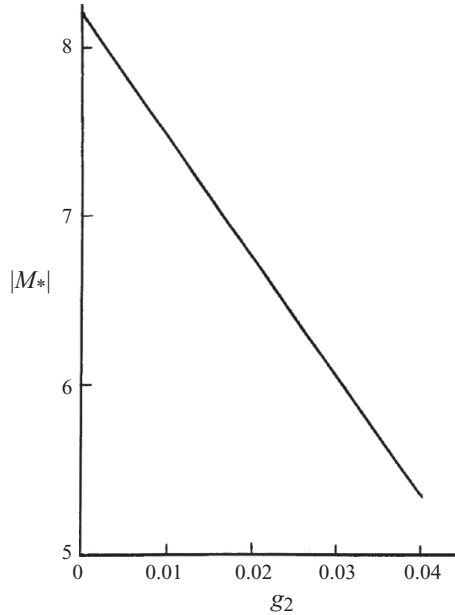
FIGURE 5. Dependence of the transition Marangoni number M_* on g_2; $g_1 = 0.02$.

appears at finite wavenumbers (figures 3a,b), becomes the strongest mode with the growth of $|M_\perp|$ (figure 3c) and finally ousts the monotonic mode of instability (figure 3d). The maximum growth rate, $\text{Re}\,\lambda_m = \max_k \text{Re}\,\lambda(k)$, and the corresponding wavenumber, k_m, are shown for both monotonic and oscillatory modes in figure 4. In the framework of the linear theory, the transition between the monotonic instability and oscillatory instability takes place at the value of the Marangoni number M_*, where the maximum growth rates of both kinds of instability are equal. The dependence of the transition Marangoni number M_* on the parameter g_2 is almost linear (see figure 5).

3.4. The case of an inclined temperature gradient

In the general case ($M_\parallel \neq 0$ and $M_\perp \neq 0$), the matrix $\boldsymbol{N}$ defined by (3.5) can be presented as

$$\boldsymbol{N} = \boldsymbol{E} + \mathrm{i}\beta\boldsymbol{D}, \tag{3.17}$$

where

$$\boldsymbol{E} = \boldsymbol{B} + \frac{M_\perp B i k^2 \kappa}{2(\kappa + Bi + Bi\kappa a)^2}\boldsymbol{C}, \;\; \beta = k_x M_\parallel. \tag{3.18}$$

The eigenvalue λ satisfies the quadratic equation

$$\lambda^2 - [\text{Tr}(\boldsymbol{E}) + \mathrm{i}\beta\text{Tr}(\boldsymbol{D})]\lambda + \det(\boldsymbol{E}) + \mathrm{i}F\beta - \beta^2 D_{11}D_{22} = 0, \tag{3.19}$$

where $F = E_{11}D_{22} + E_{22}D_{11} - E_{12}D_{21}$.

3.4.1. The case of small β

Let us present the eigenvalue λ in the form

$$\lambda = \lambda_0 + \beta\lambda_1 + \beta^2\lambda_2 + \cdots. \tag{3.20}$$
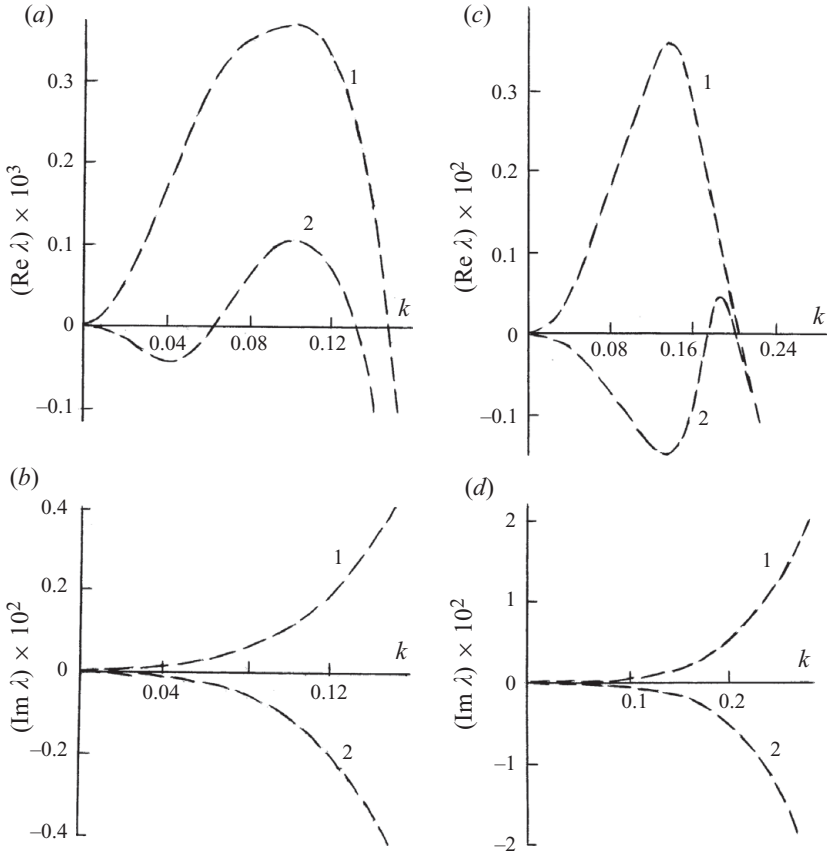
FIGURE 6. Dependences of eigenvalues λ on the wavenumber k for the waves moving to the left (lines 1) and to the right (lines 2). (a) $g_2 = 0.04$; (b) $g_2 = 0.04$; (c) $g_2 = 0.02$; (d) $g_2 = 0.02$.

In the zeroth order, we obtain the following:

$$\lambda_0^2 - \mathrm{Tr}(\boldsymbol{E})\lambda_0 + \det(\boldsymbol{E}) = 0. \tag{3.21}$$

Its solutions correspond to the case $M_\parallel = 0$ considered in the previous subsection. As we have seen, both real and complex eigenvalues are possible.

In the first order, we find that

$$2\lambda_0\lambda_1 - \lambda_1\mathrm{Tr}(\boldsymbol{E}) - i\lambda_0\mathrm{Tr}(\boldsymbol{D}) + iF = 0. \tag{3.22}$$

Hence,

$$\lambda_1 = i\frac{\lambda_0\mathrm{Tr}(\boldsymbol{D}) - F}{2\lambda_0 - \mathrm{Tr}(\boldsymbol{E})}. \tag{3.23}$$

If λ_0 is real, the first-order correction λ_1 is purely imaginary. Thus, the longitudinal component of the temperature gradient does not influence the threshold of the monotonic instability of the order $O(\beta)$. For imaginary λ_0 (on the threshold of the oscillatory instability), the correction λ_1 is complex. Note that the real part of λ_1 depends on the sign of $\mathrm{Im}\,\lambda_0$, i.e. the waves moving in opposite directions grow differently. In other words, the oscillatory neutral curve splits into two curves.
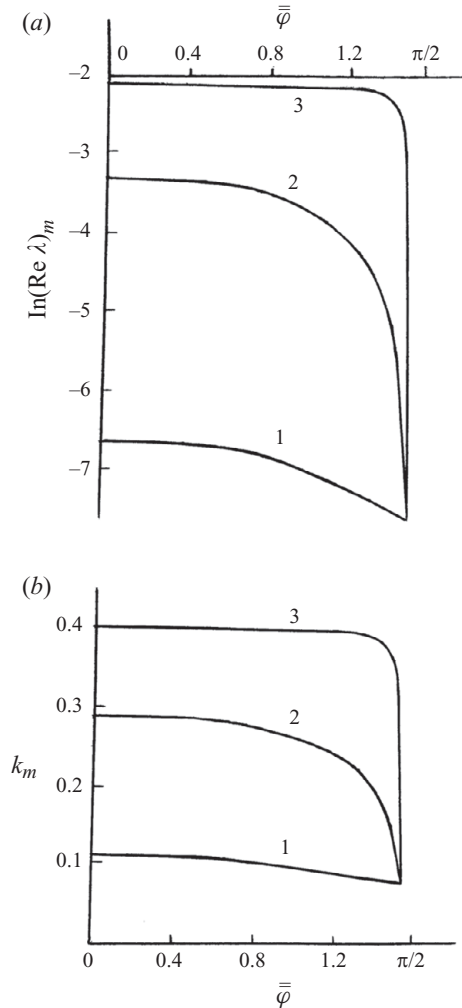
FIGURE 7. Dependence of (a) the maximum growth rate $\mathrm{Re}\,\lambda_m$ and (b) the corresponding wavenumber k_m on the angle $\bar{\bar{\varphi}}$ for $M_\| = 0.001$ (lines 1), $M_\| = 0.1$ (lines 2) and $M_\| = 5$ (lines 3). Other parameters: $M_\perp = -5$, $g_1 = 0.02$ and $g_2 = 0.04$.

Similarly, the second-order correction λ_2 can be calculated:

$$\lambda_2 = \frac{-\lambda_1^2 + i\lambda_1 \mathrm{Tr}(\boldsymbol{D}) + D_{11}D_{22}}{2\lambda_0 - \mathrm{Tr}(\boldsymbol{E})}. \tag{3.24}$$

Note that it is purely real for a monotonic mode (when λ_0 is real and λ_1 is imaginary). The predictions presented above are illustrated by the numerical computation of the eigenvalues for the same set of parameter as in figure 3(c), but with $M_\| = 10^{-4}$ (see figures 6a,b). Comparing figures 6(a) and 3(c), one can see that for values of k where the instability is monotonic at $M_\| = 0$, the change of the growth rate $\mathrm{Re}\,\lambda$ is small. In the region of k, where the instability is oscillatory at $M_\| = 0$, the growth rate of the waves moving to the left ($\mathrm{Im}\,\lambda > 0$, lines 1) is significantly higher than that of the waves moving to the right ($\mathrm{Im}\,\lambda < 0$, lines 2). With the decrease of the parameter g_2, all the lines keep their shape, but the growth rate becomes much larger (see figures 6c and 6d).
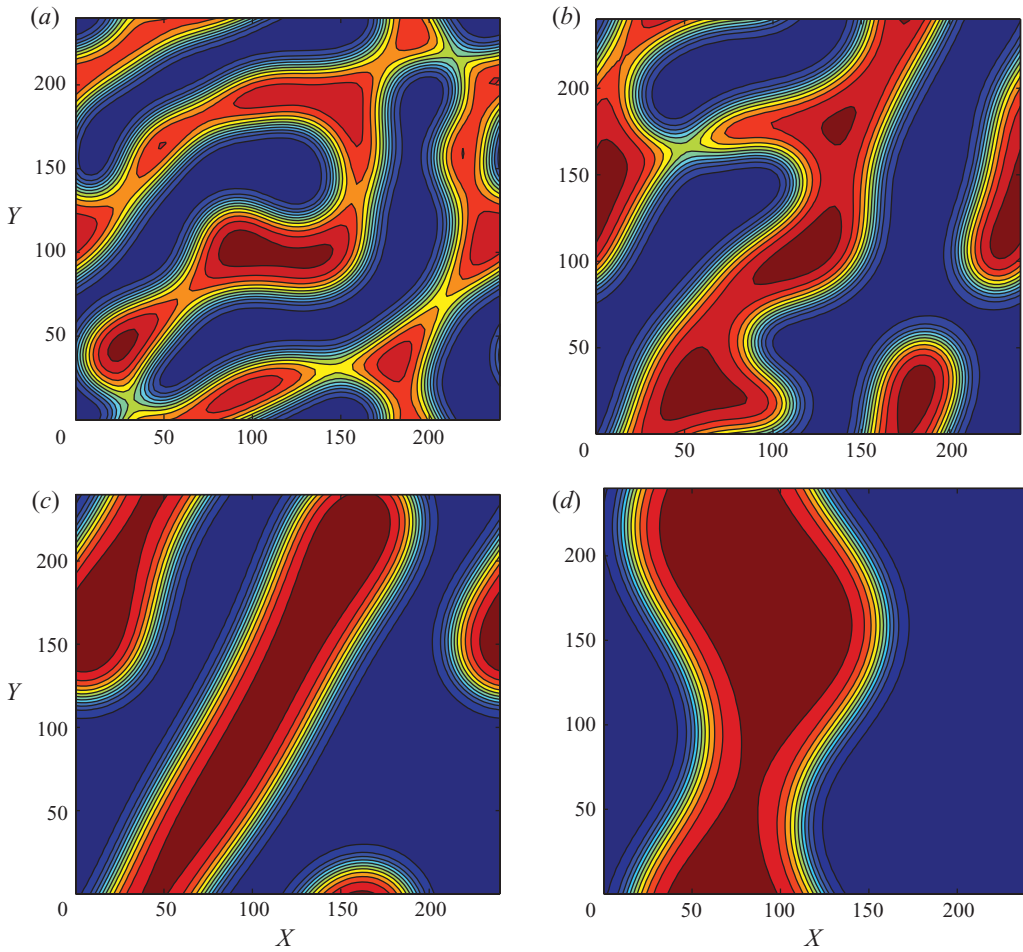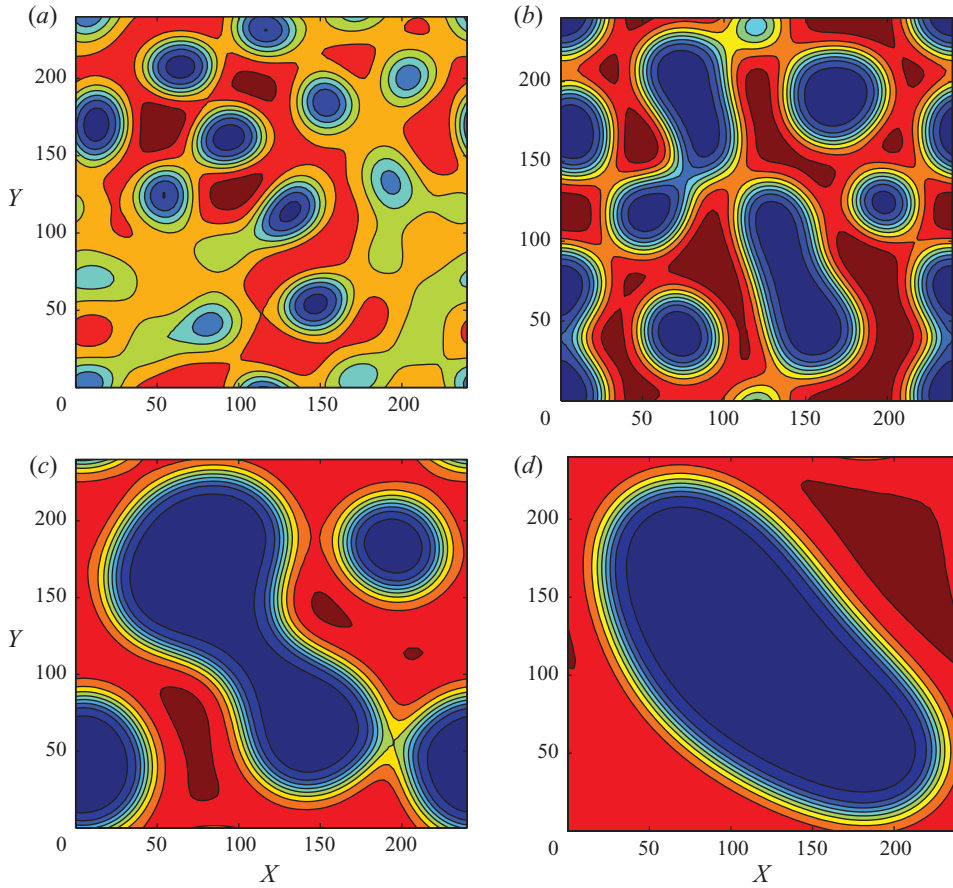
FIGURE 8. (Colour online) Isolines of $\tilde{h}_2(X, Y, \tau)$: (a) $\tau = 20\,000$; (b) $\tau = 40\,000$; (c) $\tau = 120\,000$; (d) $\tau = 360\,000$. $M_\perp = M_\parallel = 0$; $g_1 = 0.02$; $g_2 = 0.03$; other parameters are given in the text.

3.4.2. *The case of large β*

This case corresponds to a strong longitudinal temperature gradient ($M_\parallel$ is sufficiently large) and a disturbance orientation not close to a longitudinal one (k_x is not small). The solution of (3.19) can be written as

$$\lambda = \lambda_{-1}\beta + \lambda_0 + \cdots. \tag{3.25}$$

For λ_{-1}, we obtain the following quadratic equation:

$$\lambda_{-1}^2 - i\lambda_{-1}\mathrm{Tr}(\boldsymbol{D}) - D_{11}D_{22} = 0. \tag{3.26}$$

We find that the roots are

$$\lambda_{-1}^+ = iD_{11}, \quad \lambda_{-1}^- = iD_{22}. \tag{3.27}$$

Thus, the corresponding terms in the expansion (3.25) are purely imaginary and do not influence the stability. The term λ_0 is obtained from the relation

$$2\lambda_0\lambda_{-1} - \lambda_{-1}\mathrm{Tr}(\boldsymbol{E}) - i\lambda_0\mathrm{Tr}(\boldsymbol{D}) + iF = 0. \tag{3.28}$$
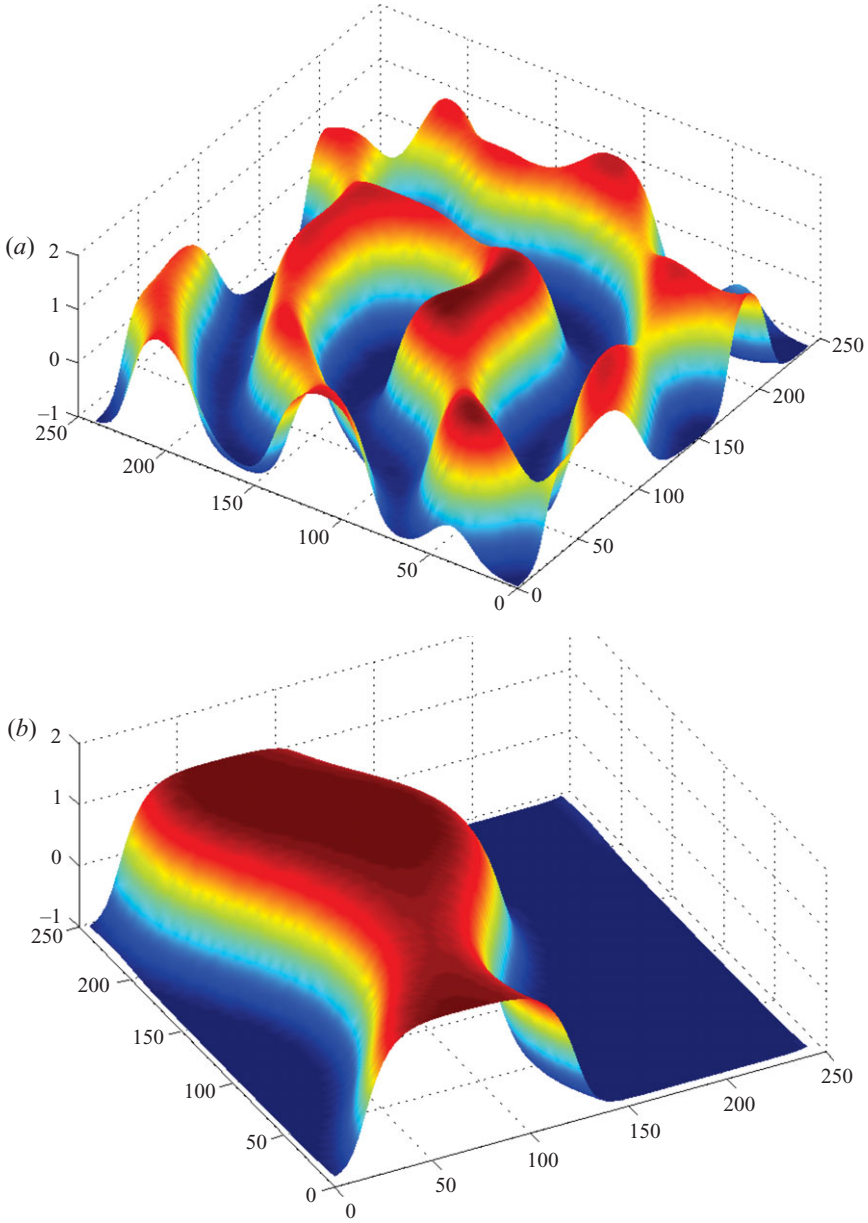
FIGURE 9. (Colour online) Shapes of the free surface, $\tilde{h}_2(X, Y, \tau)$: (a) $\tau = 20\,000$;
(b) $\tau = 360\,000$; other parameters are as in figure 8.

Hence,

$$\lambda_0^+ = \frac{D_{11}\mathrm{Tr}(\boldsymbol{E}) - F}{D_{11} - D_{22}}, \quad \lambda_0^- = \frac{D_{22}\mathrm{Tr}(\boldsymbol{E}) - F}{D_{22} - D_{11}} \tag{3.29}$$

are real.

Therefore, the growth rates

$$\mathrm{Re}\,\lambda^\pm = \lambda_0^\pm + o(1), \tag{3.30}$$

FIGURE 10. (Colour online) Fields of $\tilde{h}_2(X, Y, \tau)$: (a) $\tau = 20\,000$; (b) $\tau = 40\,000$; (c) $\tau = 120\,000$; (d) $\tau = 360\,000$. $M_\perp = M_\parallel = 0$; $g_1 = 0.02$; $g_2 = 0.04$; other parameters are given in the text.

i.e. they do not depend on the orientation of the wave vector and on the longitudinal Marangoni number $M_\parallel$. (Although the elements of matrix $\boldsymbol{D}$, which is related to the longitudinal temperature gradient, are significant).

We come to the conclusion that for sufficiently large $M_\parallel$, on the linear stage of the instability development, any disturbances grow or decay independently on the orientation of their wave vectors, except the disturbances with small k_x (nearly longitudinal disturbances).

Thus, we arrive at the following paradoxical situation. The longitudinal component of the temperature gradient is the only factor that violates the rotational symmetry of the problem. However, when this component is sufficiently large, the isotropy of the problem is partially restored (the real part of the growth rate depends only on k^2 and not on k_x to the leading order, while the imaginary part keeps its dependence on k_x), except the region of nearly longitudinal structures that have small β, even for large $M_\parallel$.

The predictions presented above are confirmed by direct computations (see figure 7a). For a fixed direction of the wave vector, determined by the angle $\varphi = \tan^{-1}(k_y/k_x)$, we have found the maximum growth rate

$$(\text{Re}\,\lambda)_m(\varphi) = \max_k (\text{Re}\,\lambda)(k\cos\varphi, k\sin\varphi). \tag{3.31}$$
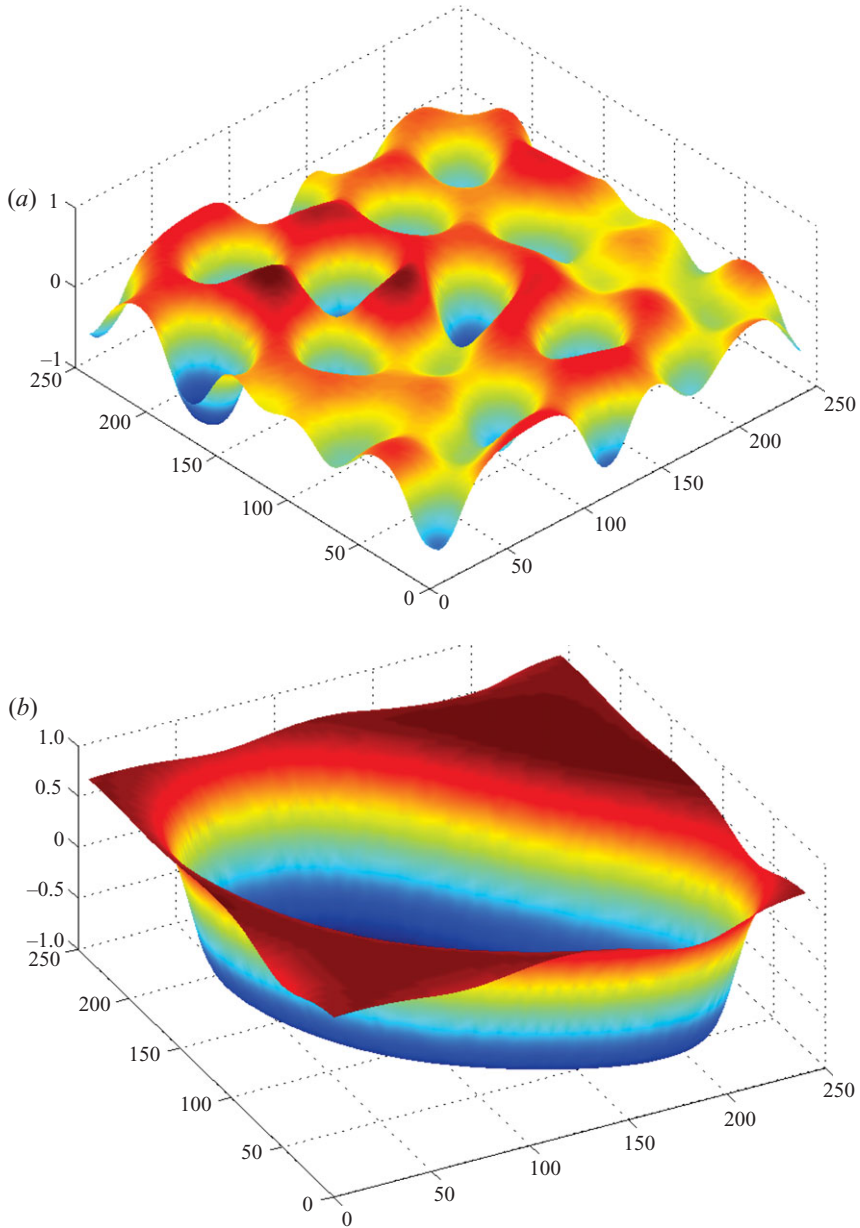
FIGURE 11. (Colour online) Shapes of the free surface, $\tilde{h}_2(X, Y, \tau)$: (*a*) $\tau = 20\,000$; (*b*) $\tau = 360\,000$; other parameters are as in figure 10.

The value $(\operatorname{Re}\lambda)_m(\pm\pi/2)$ does not depend on $M_\parallel$. For relatively small $M_\parallel$, the maximum growth rate depends significantly on the orientation of the wave vector (lines 1 and 2). With the growth of $M_\parallel$, a long 'plateau' is developed (lines 3): the maximum growth rate is nearly constant and decreases rapidly when φ approaches $\pm\pi/2$. Note that $(\operatorname{Re}\lambda)_m(0) > (\operatorname{Re}\lambda)_m(\pi/2)$, i.e. the disturbance with a longitudinal orientation grows slower than any other disturbances. The dependences of the wavenumber $k_m(\varphi)$ corresponding to the maximum growth rate are similar (see figure 7*b*).

(*a*)

(*b*)

(*c*)
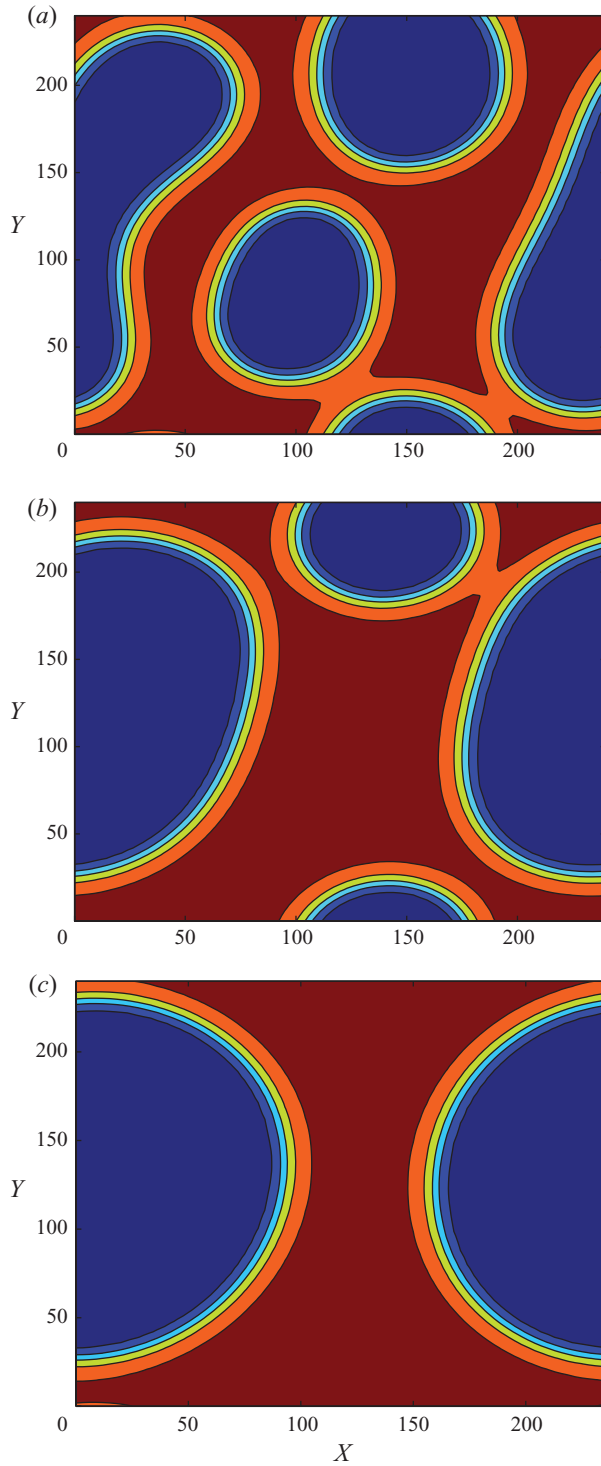
FIGURE 12. (Colour online) Fields of $\tilde{h}_2(X, Y, \tau)$: (*a*) $\tau = 40\,000$; (*b*) $\tau = 120\,000$; (*c*) $\tau = 240\,000$. $M_\perp = -1$; $M_\parallel = 0$; $g_1 = 0.02$; $g_2 = 0.04$; other parameters are given in the text.
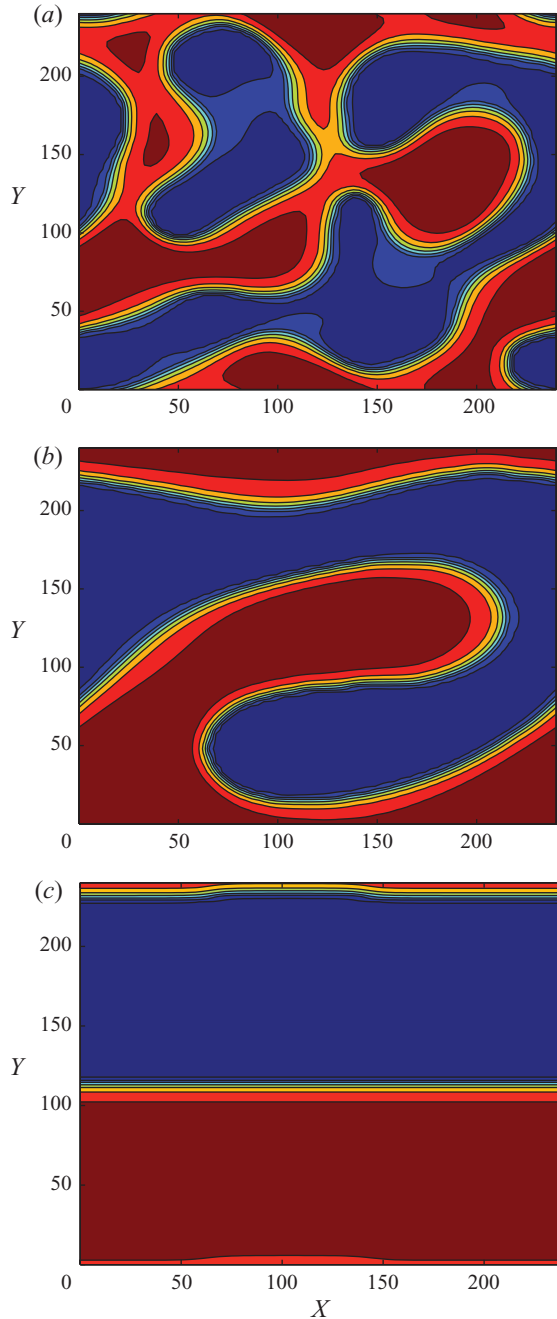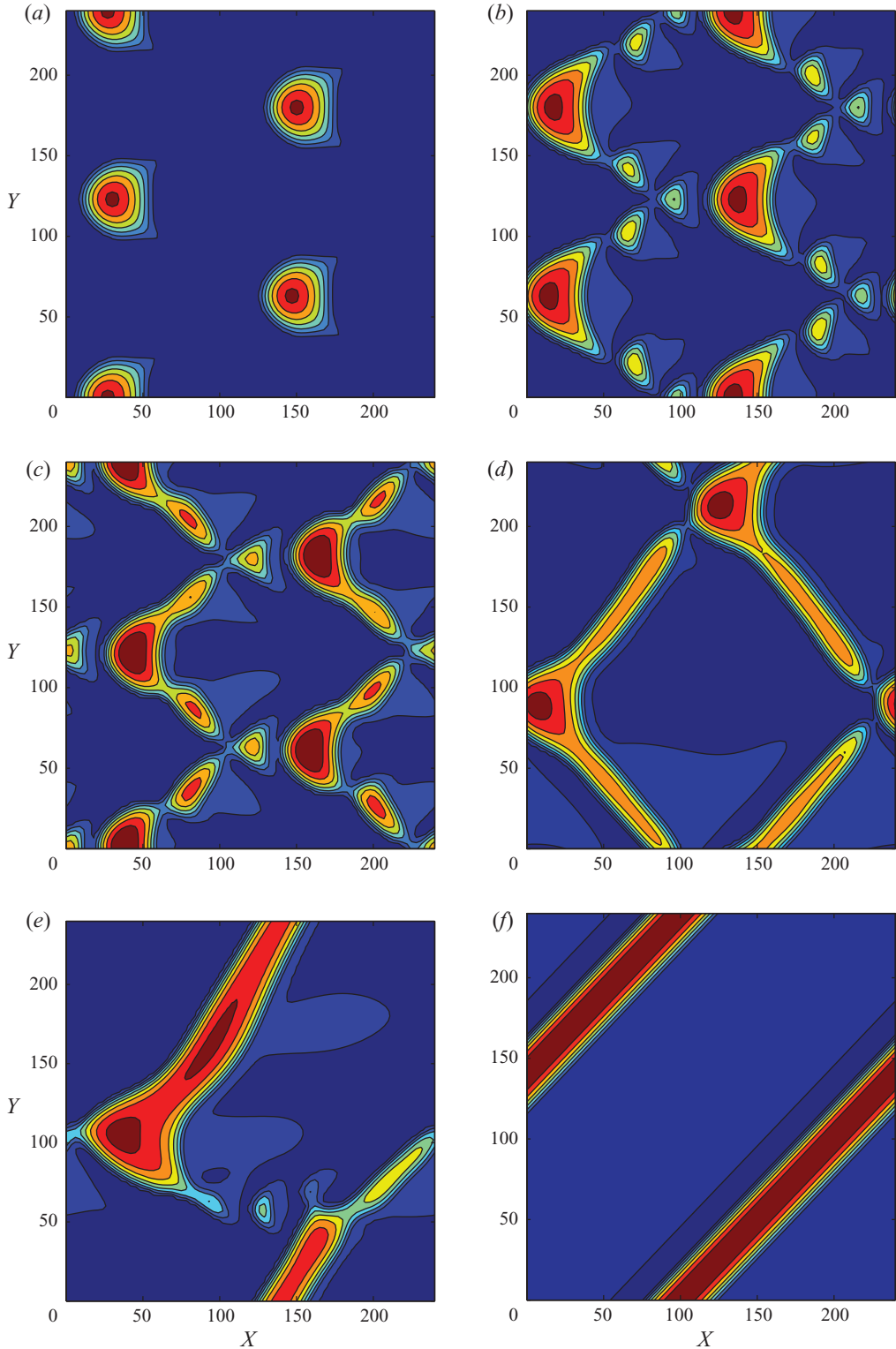
FIGURE 13. (Colour online) Fields of $\tilde{h}_2(X, Y, \tau)$: (a) $\tau = 6500$; (b) $\tau = 20\,000$; (c) $\tau = 120\,000$. $M_\perp = -5$; $M_\parallel = 0$; $g_1 = 0.02$; $g_2 = 0.04$; other parameters are given in the text.

4. Nonlinear simulations

Evolution equations (2.36) have been discretized by central differences for spatial derivatives and solved using an explicit scheme. Periodic boundary conditions have been applied on the boundaries of the computational region. Initial conditions for h_j, $j = 1, 2$, have been chosen in such a way that the mean value of $h_1(X, Y, 0)$ was

FIGURE 14. (Colour online) Fields of $\tilde{h}_2(X, Y, \tau)$: (*a*) $\tau = 48\,800$; (*b*) $\tau = 50\,150$; (*c*) $\tau = 51\,100$; (*d*) $\tau = 62\,100$; (*e*) $\tau = 72\,800$; (*f*) $\tau = 96\,200$. $M_\perp = -5$; $M_\parallel = 0.1$; (*a*) $g_1 = g_2 = 0$; (*b*)–(*f*) $g_1 = 0.04$, $g_2 = 0.02$; other parameters are given in the text.
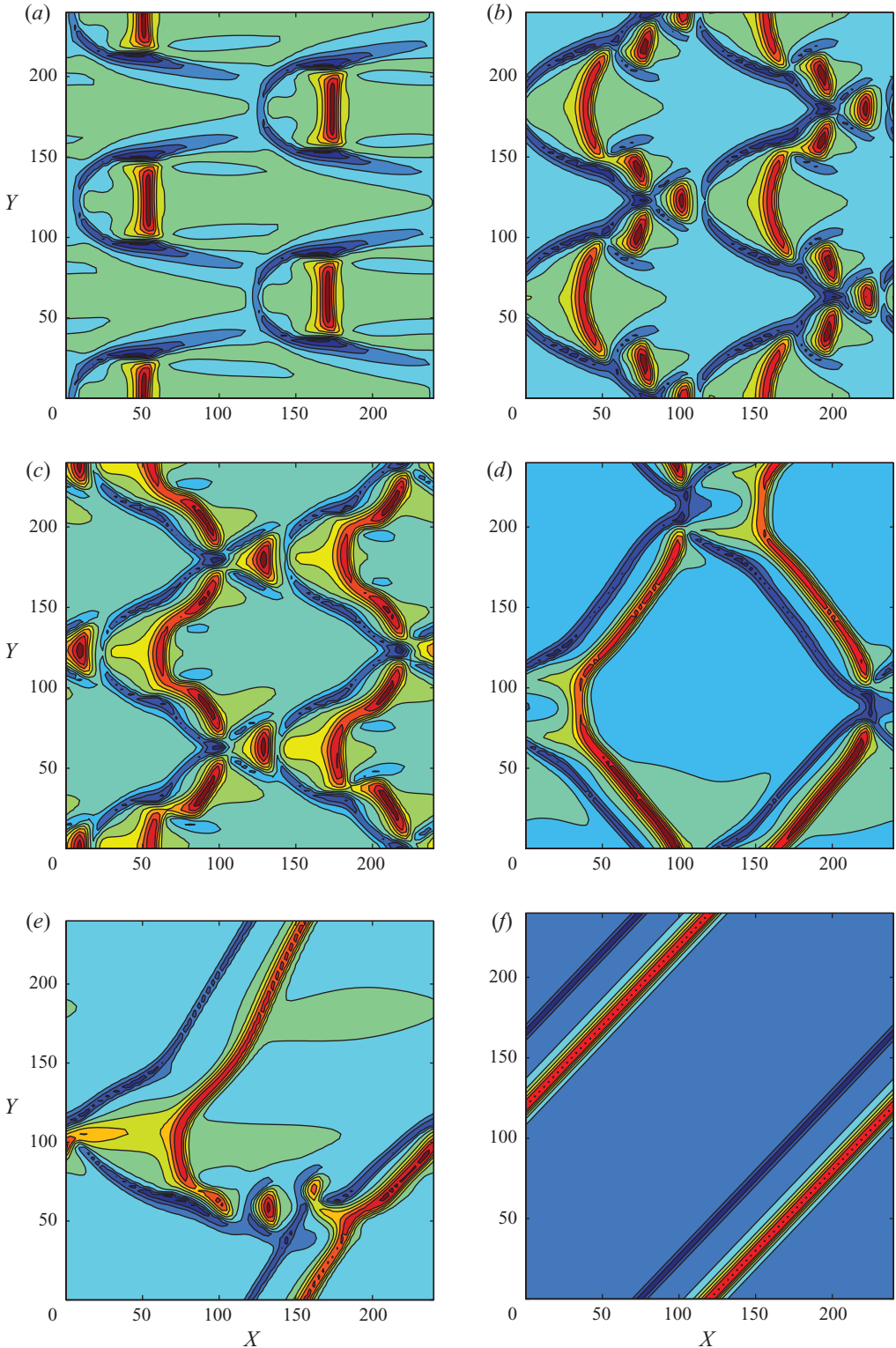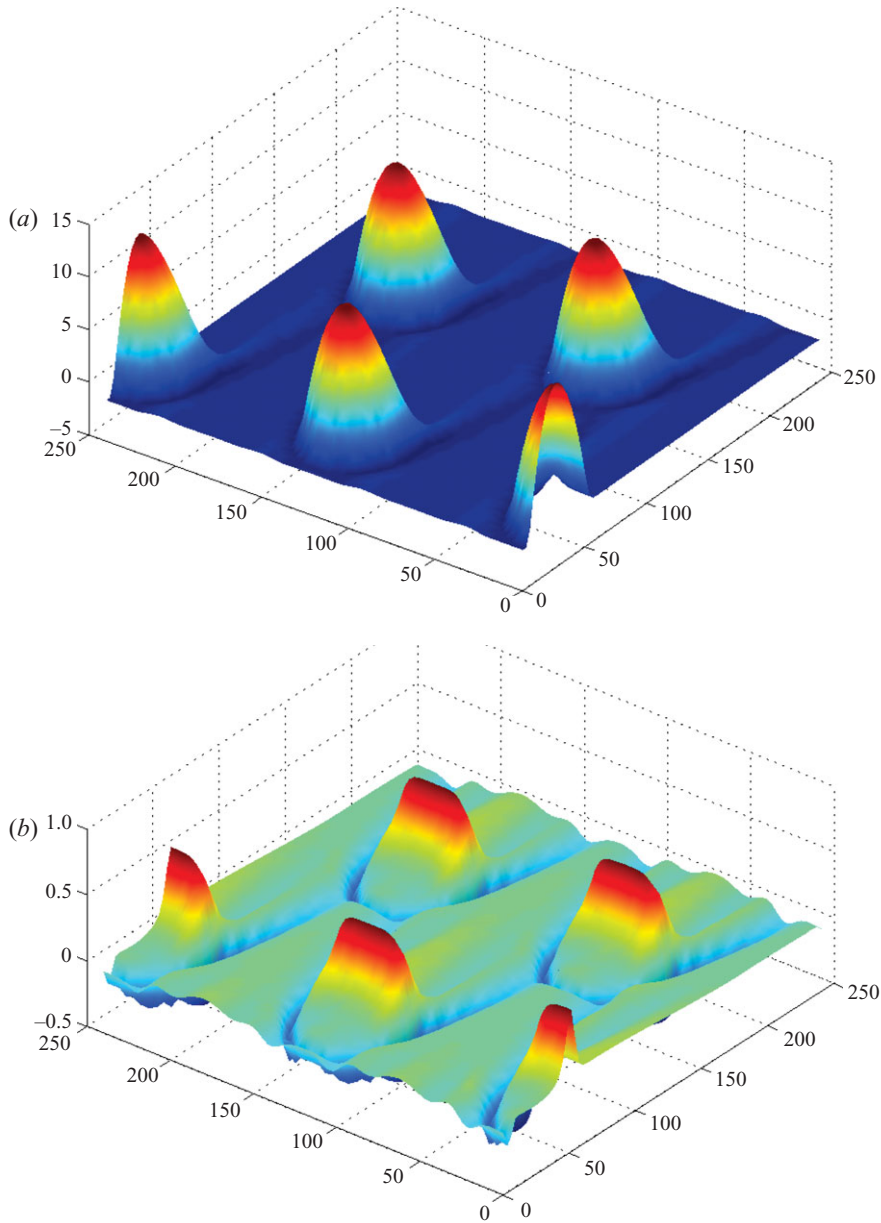
FIGURE 15. (Colour online) Fields of $\tilde{h}_1(X, Y, \tau)$: (*a*) $\tau = 48\,800$; (*b*) $\tau = 50\,150$; (*c*) $\tau = 51\,100$; (*d*) $\tau = 62\,100$; (*e*) $\tau = 72\,800$; (*f*) $\tau = 96\,200$. $M_\perp = -5$; $M_\parallel = 0.1$; (*a*) $g_1 = g_2 = 0$; (*b*)–(*f*) $g_1 = 0.04$, $g_2 = 0.02$; other parameters are given in the text.

FIGURE 16. (Colour online) Shapes of interfaces at $\tau = 48\,800$: (a) $\tilde{h}_2(X, Y, \tau)$; (b) $\tilde{h}_1(X, Y, \tau)$. $g_1 = g_2 = 0$; other parameters are given in the text.

equal to 1 and the mean value of $h_2(X, Y, 0)$ was equal to h, where $h > 1$. Hence, our computations depend on the additional geometric parameter $h = H_2^0/H_1^0$. Small random deviations of $h_j(X, Y, 0)$ from their mean values were imposed using a code, creating pseudo-random numbers. The computations have been performed in the region 240×240 using the grid 400×400 for the following values of parameters: $\eta = 1.2$, $\kappa = 1$, $\alpha = 1$ and $h = 2.5$.
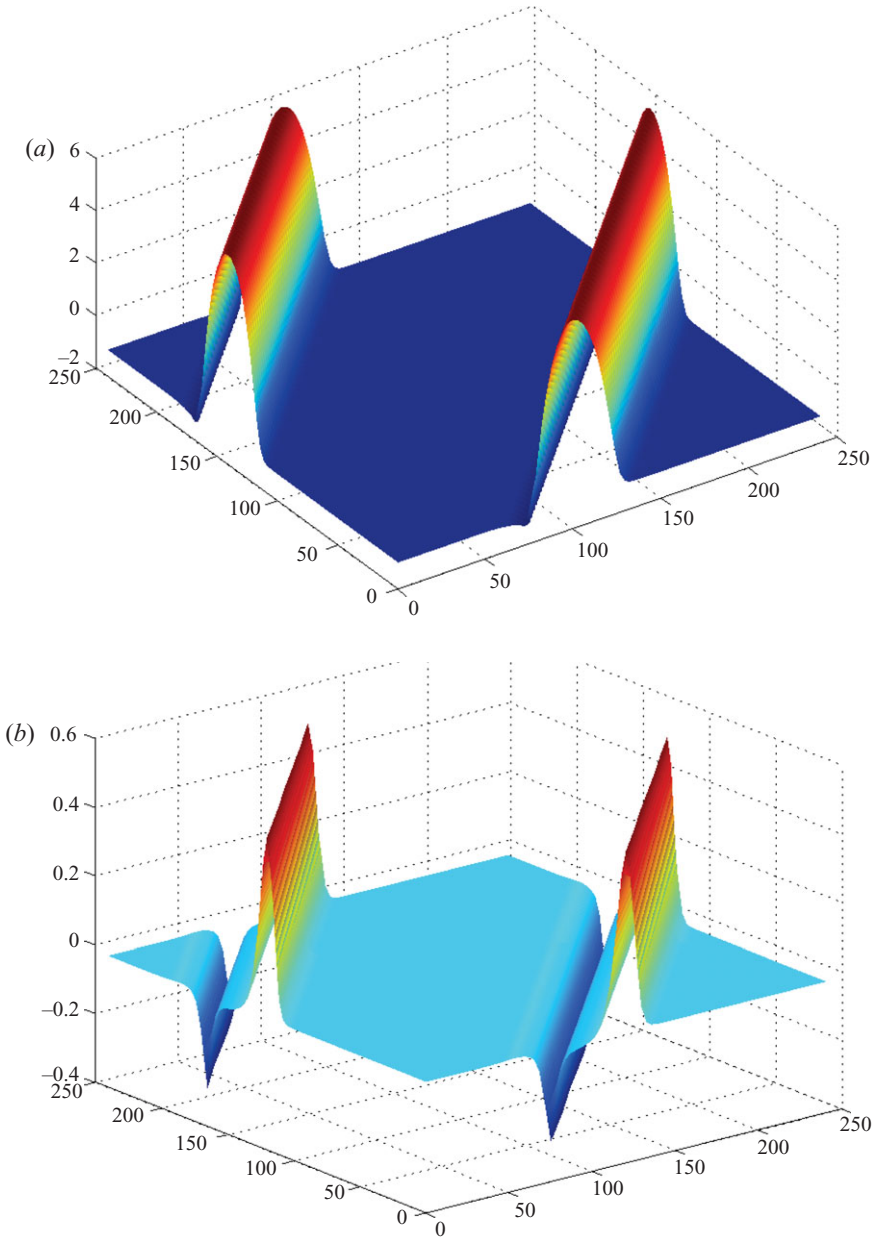
FIGURE 17. (Colour online) Shapes of interfaces at $\tau = 96\,200$: (a) $\tilde{h}_2(X, Y, \tau)$; (b) $\tilde{h}_1(X, Y, \tau)$. $g_1 = 0.04$, $g_2 = 0.02$; other parameters are given in the text.

4.1. *Coarsening regimes*

First, let us recall the results of simulations done by Fisher & Golovin (2005) in the case where $a_0 = 1$, $a_1 = -0.4$, $a_2 = -0.1$; $M_\perp = M_\parallel = 0$; and $g_1 = g_2 = 0$. As was explained in §3, this choice corresponds to an attraction between the outer interfaces and to a repulsion between the adjacent interfaces. The attraction is the origin of an instability, while the repulsion prevents the rupture of the film. Due to the interplay of both types of interactions, the film is separated into two phases: a number of relatively
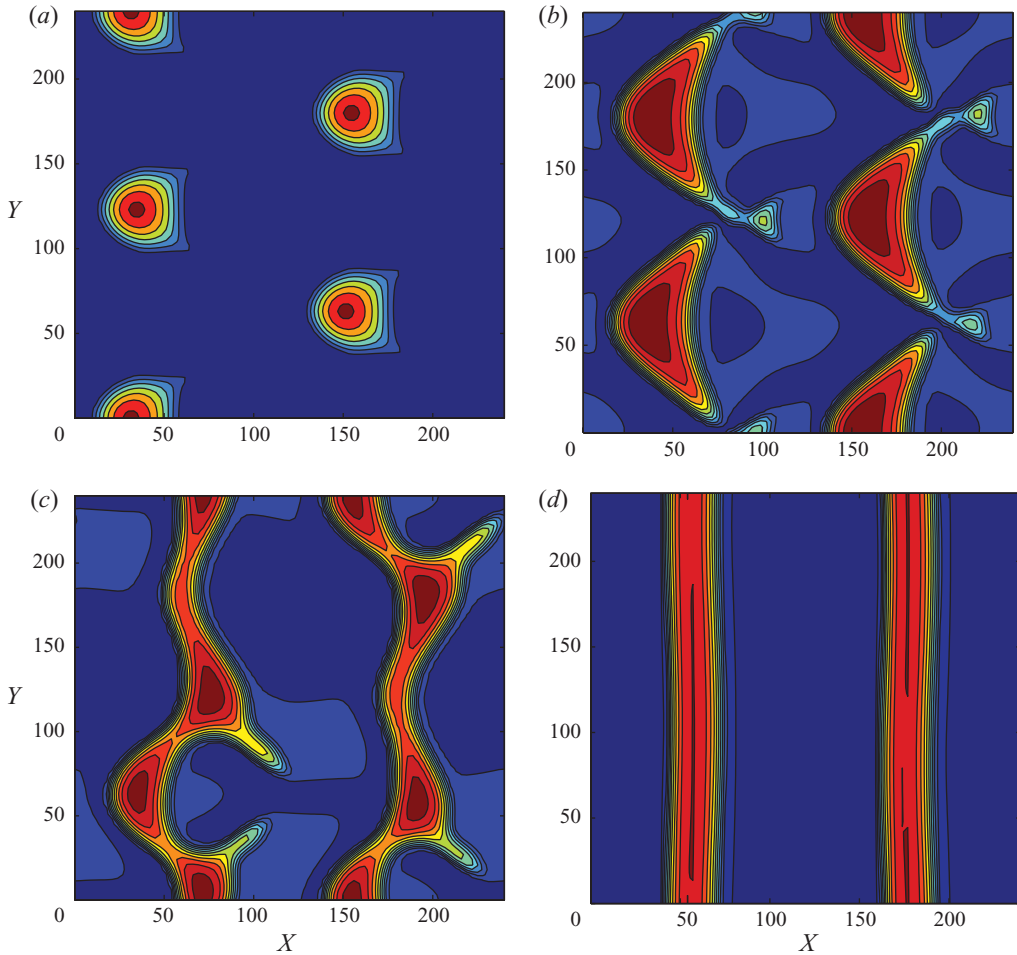
FIGURE 18. (Colour online) Fields of $\tilde{h}_2(X, Y, \tau)$: (a) $\tau = 59\,080$; (b) $\tau = 61\,140$; (c) $\tau = 62\,900$; (d) $\tau = 78\,980$. $M_\perp = -5$; $M_\parallel = 0.1$; (a) $g_1 = g_2 = 0$; (b)–(d) $g_1 = 0.02$, $g_2 = 0.04$; other parameters are given in the text.

thick 'droplets' of a parabolic shape and a relatively thin 'precursor' film between the 'droplets'. Let us emphasize that the repulsive interaction keeps the thickness of the 'thin film' macroscopic; therefore, it can be described within the continuum approach. No true rupture of the film and the formation of a contact line take place. (For the description of the above-mentioned phenomena beyond the approach used in the present paper, see Shikhmurzaev 2008.) Let us also note that the horizontal size of 'droplets' is large in comparison to their height; hence, the apparent 'contact angle' is very small. Therefore, the separation of the film into the phases does not violate the validity conditions of the lubrication approximation.

In the framework of the linear stability theory, the major factor is the stabilizing effect of the parameter g_2, while the influence of the density stratification parameter $g_1 - g_2$ is much weaker (see §3). With the growth of g_1 and g_2, the coefficient in the weakly nonlinear amplitude equation, which is responsible for the nonlinear development of disturbances, diminishes and then changes its sign (see figure 10 in Fisher & Golovin 2005). This is a cause of the replacement of droplets by 'labyrinths' and then by hole-like disturbances. Our strongly nonlinear simulations
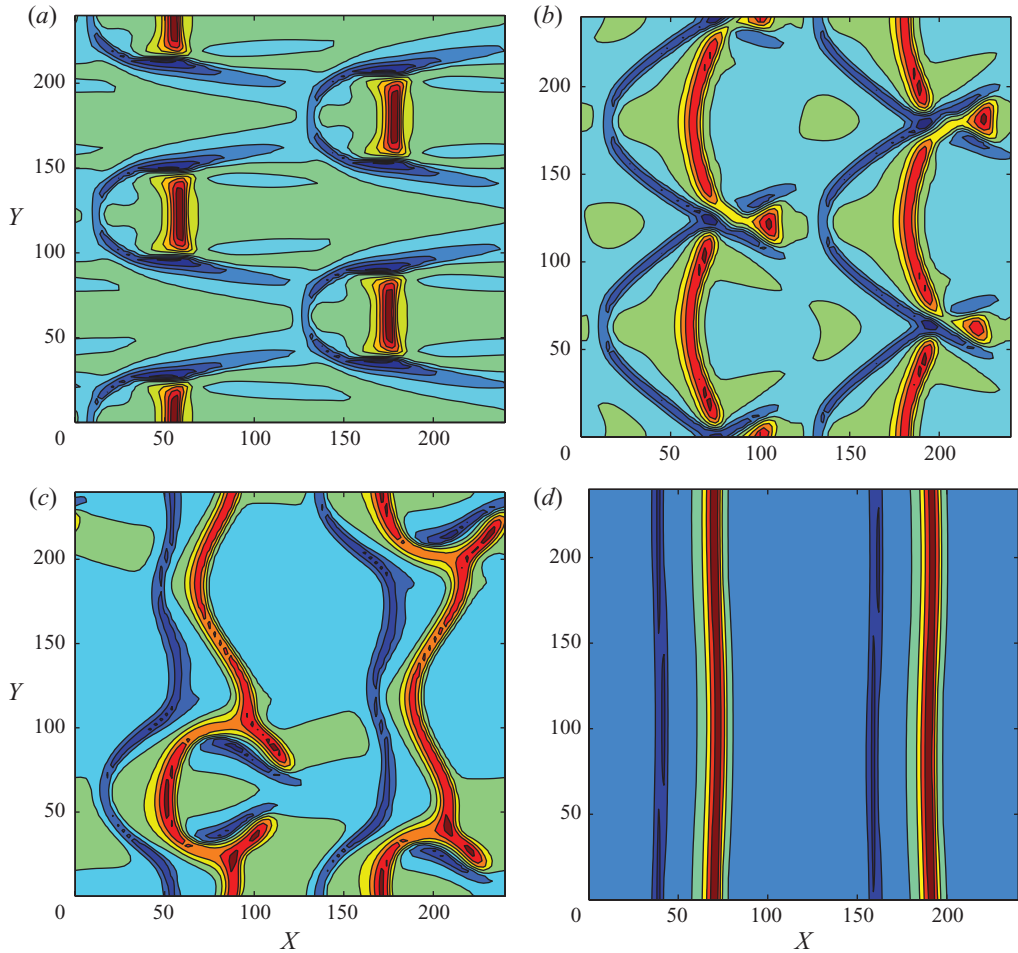
FIGURE 19. (Colour online) Fields of $\tilde{h}_1(X, Y, \tau)$: (a) $\tau = 59\,080$; (b) $\tau = 61\,140$; (c) $\tau = 62\,900$; (d) $\tau = 78\,980$. $M_\perp = -5$; $M_\parallel = 0.1$; (a) $g_1 = g_2 = 0$; (b)–(d) $g_1 = 0.02$, $g_2 = 0.04$; other parameters are given in the text.

have confirmed that prediction. Indeed, for $g_1 = 0.02$ and $g_2 = 0.03$, the droplets are not developed anymore. Instead of them, one observes a structure where both elevations and depressions are present. (See figure 8, where snapshots for the field of $\tilde{h}_2(X, Y, \tau) = h_2(X, Y, \tau) - h$ are shown.) The three-dimensional plots of $\tilde{h}_2(X, Y, \tau)$ are shown in figure 9. Let us note that the horizontal scale and the vertical scale in figure 9 (and in other similar figures below) are strongly different; although the elevations and depressions look steep, they are actually very sloping; therefore, the shapes of the interfaces are within the validity region of the lubrication approximation. For even larger values of g_2 ($g_2 = 0.04$), a big hole develops on the free surface and on the interface (see figure 10). In the latter case, the three-dimensional plots of $\tilde{h}_2(X, Y, \tau)$ are shown in figure 11.

In accordance with the predictions of the linear theory, a heating from above ($M_\perp < 0$) strengthens the instability for the value $Bi = 10$. On the nonlinear stage, a faster coarsening of holes and the enhancement of the holes depth are observed (see figure 12). For even larger $M_\perp$, the symmetry between depressions and elevations is restored; therefore, neither holes nor droplets are formed (see figures 13a,b). Finally,
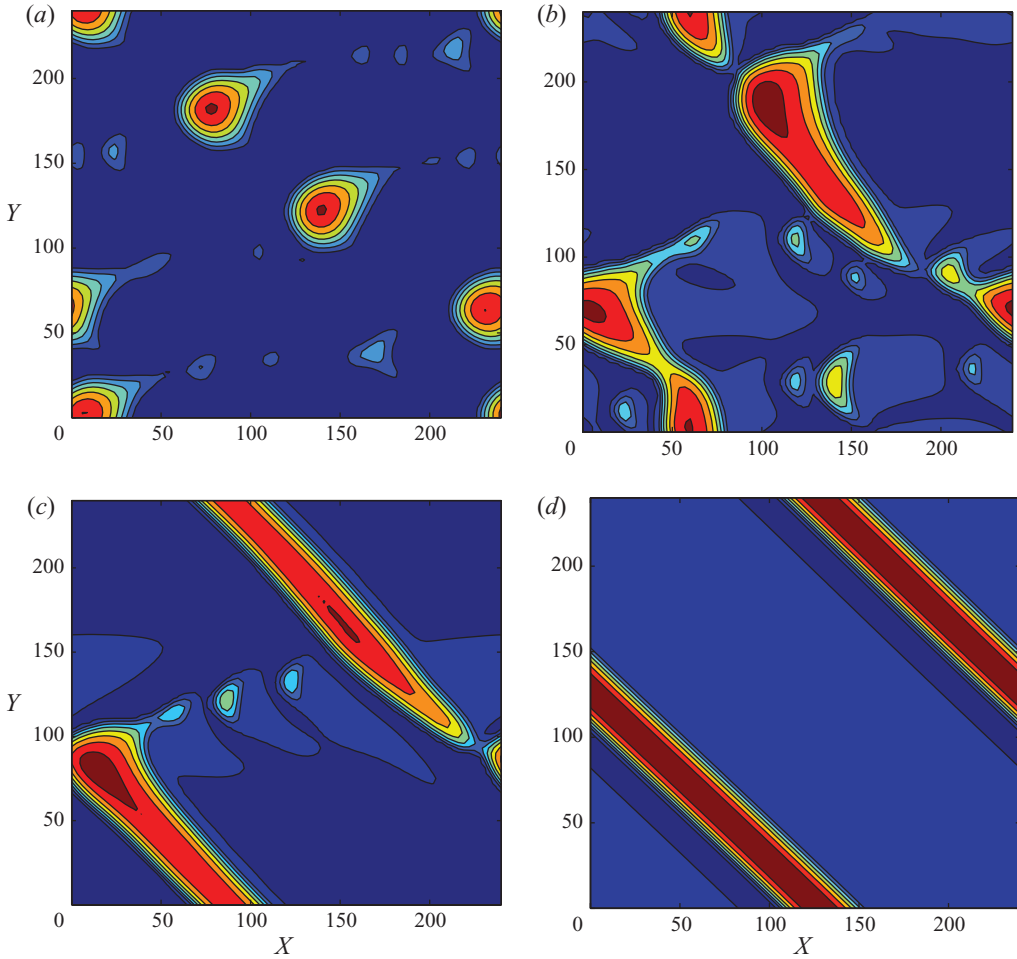
FIGURE 20. (Colour online) Fields of $\tilde{h}_2(X, Y, \tau)$: (a) $\tau = 59\,200$; (b) $\tau = 64\,360$; (c) $\tau = 67\,840$; (d) $\tau = 78\,880$. $M_\perp = -5$; $M_\parallel = 0.11$; (a) $g_1 = g_2 = 0$; (b)–(d) $g_1 = 0.04$, $g_2 = 0.02$; other parameters are given in the text.

a one-dimensional structure is developed that resembles a kink–antikink pair of the pure Cahn–Hilliard equation (see figure 13c).

4.2. *Wavy patterns*

Coarsening is not the only scenario of the nonlinear development of instabilities. In a definite region of parameters, the coarsening can been stopped, and finally, an ordered or disordered system of droplets/holes is created, which never coalesce into a sole droplet/hole (Nepomnyashchy & Simanovskii 2008). In the absence of gravity ($g_1 = g_2 = 0$), an ordered structure of equally sized droplets moving with equal velocities and located at equal distances from each other has been observed at $M_\perp = -5$ and $M_\parallel = 0.1$ (see figures 14a and 15a). Let us emphasize that the ordered droplets system is not a result of a casual monodispersity of droplets due to a specific choice of initial conditions, but a result of a natural evolution of the system to its stable configuration. The same ordered system of droplets has been obtained from different initial conditions. Under the action of the gravity force ($g_1 = 0.04$ and $g_2 = 0.02$), the ordered system of droplets is destroyed and transforms through intermediate
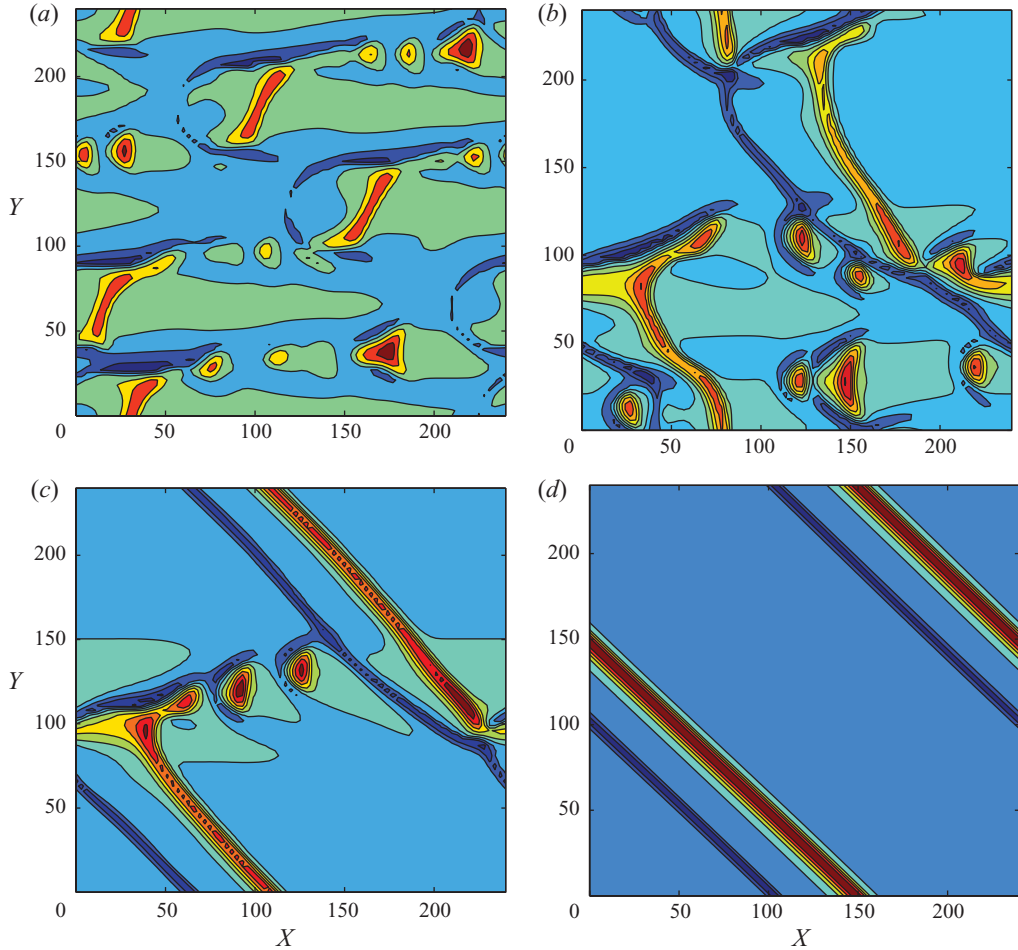
FIGURE 21. (Colour online) Fields of $\tilde{h}_1(X, Y, \tau)$: (a) $\tau = 59\,200$; (b) $\tau = 64\,360$; (c) $\tau = 67\,840$; (d) $\tau = 78\,880$. $M_\perp = -5$; $M_\parallel = 0.11$; (a) $g_1 = g_2 = 0$; (b)–(d) $g_1 = 0.04$, $g_2 = 0.02$; other parameters are given in the text.

stages (figures 14b–e and 15b–e) to a new stable configuration of a one-dimensional waves (figures 14f and 15f), moving in the direction inclined with respect to the direction of the horizontal temperature gradient (from the right to the left). The shapes of $\tilde{h}_2(X, Y, \tau)$ and $\tilde{h}_1(X, Y, \tau)$ are shown in figures 16 (for $g_1 = g_2 = 0$) and 17 (for $g_1 = 0.04$ and $g_2 = 0.02$).

Another possible scenario of the destruction of the ordered droplets system takes place under the action of the inverted values of g_1 and g_2 ($g_1 = 0.02$ and $g_2 = 0.04$). In this case, the ordered system of droplets transforms into a one-dimensional wave, moving parallel to the horizontal temperature gradient (from the right to the left); see figures 18 and 19.

Similar final wavy patterns are obtained for $M_\perp = -5$ and $M_\parallel = 0.11$, where in the absence of gravity ($g_1 = g_2 = 0$), a disordered system of droplets is observed. For $g_1 = 0.04$ and $g_2 = 0.02$, the evolution leads to a system of one-dimensional waves with the fronts inclined to the direction of the horizontal temperature gradient (figures 20 and 21), while for $g_1 = 0.02$ and $g_2 = 0.04$, the wave fronts are transverse to its direction (figure 22).
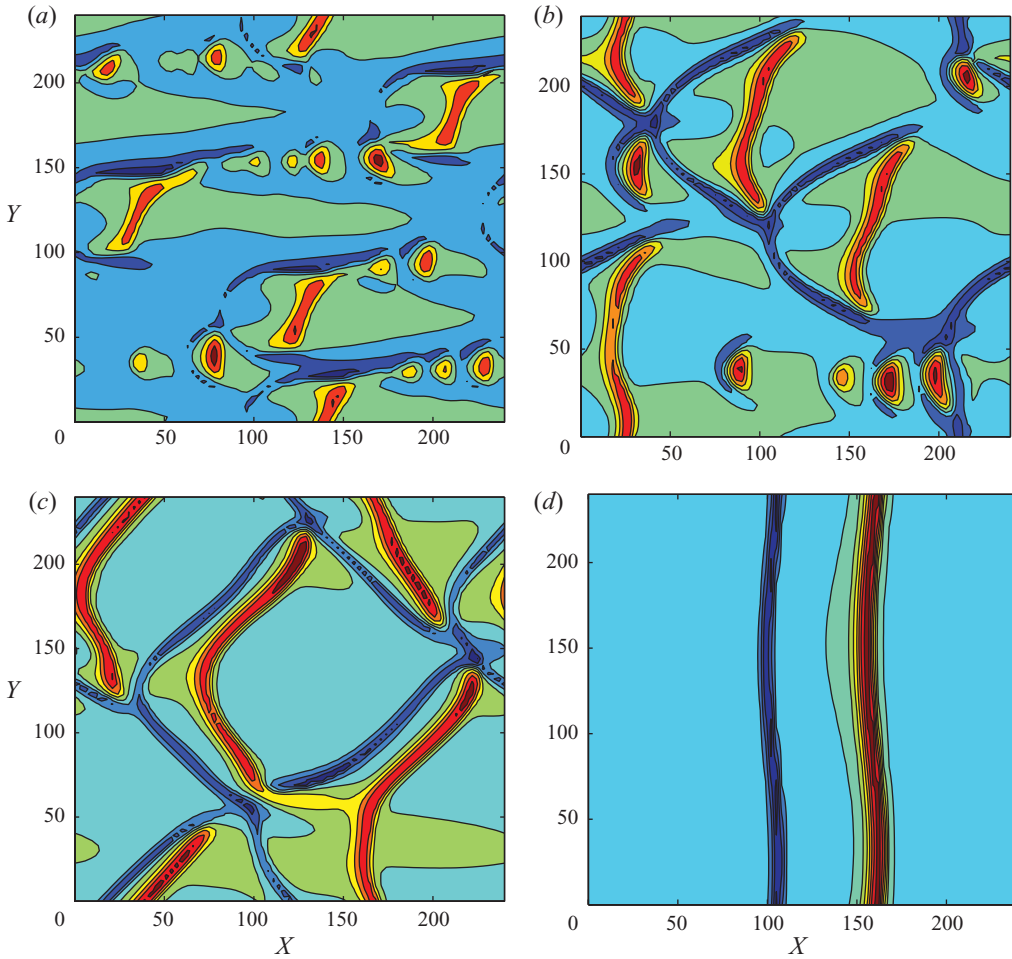
FIGURE 22. (Colour online) Fields of $\tilde{h}_1(X, Y, \tau)$: (a) $\tau = 59\,360$; (b) $\tau = 60\,520$; (c) $\tau = 62\,280$; (d) $\tau = 78\,360$. $M_\perp = -5$; $M_\parallel = 0.11$; (a) $g_1 = g_2 = 0$; (b)–(d) $g_1 = 0.02$, $g_2 = 0.04$; other parameters are given in the text.

5. Conclusions

The novelty of the present investigation compared to the existing literature is in the analysis of the influence of the gravity on the instabilities of non-isothermic two-layer films by means of the long-wave approach. A system of nonlinear evolution equations, which takes into account the van der Waals forces and the thermocapillary effect, is derived. It has been found that the influence of the upper fluid density, characterized by the parameter g_2, is stronger than that of the difference of fluid densities, characterized by the parameter $g_1 - g_2$. The vertical temperature gradient may create a transition from the monotonic instability, which is mostly due to the van der Waals forces, to an oscillatory instability, caused mostly by the thermocapillary effect. In a contradistinction to one-layer systems, the horizontal component of the temperature gradient strongly influences the instability growth rate; this influence is especially strong in the case of an oscillatory instability. With the growth of the horizontal temperature gradient, the isotropy of the growth rate is restored, except a small interval of inclination angles for the wave vector. The gravity also influences

the nonlinear stage of the disturbances development. Specifically, one can observe formation of stripes or holes instead of droplets. In the case of wavy patterns, the gravity leads to the simplification of the patterns' structures. A novel effect is the transformation of the two-dimensional ordered and disordered wavy patterns into one-dimensional waves with the fronts inclined or transverse to the direction of the horizontal temperature gradient.

Finally, let us discuss the observability of the phenomena described above. Using the estimates $H_1^0 \sim 100$ nm and $L^* \sim 20$ μm, we come to the conclusion that a typical value of the parameter $M_\perp \sim 5$ corresponds to the case $\alpha_1(T_s - T_g)/\sigma_1^0 \sim 10^{-4}$, i.e. the characteristic temperature differences sufficient for the development of the above-mentioned regimes are about 10^{-2} K. Hence, even a very weak heating of the film can create an instability.

REFERENCES

BANDYOPADHYAY, D., GULABANI, R. & SHARMA, A. 2005 Instability and dynamics of thin liquid bilayers. *Ind. Engng Chem. Res.* **44**, 1259.

BANDYOPADHYAY, D. & SHARMA, A. 2006 Nonlinear instabilities and pathways of rupture in thin liquid bilayers. *J. Chem. Phys.* **125**, 054711.

COLINET, P., JOANNES, L., IORIO, C. S., HAUT, B., BESTEHORN, M., LEBON, G. & LEGROS, J. C. 2003 Interfacial turbulence in evaporating liquids: theory and preliminary results of the ITEL-Master 9 sounding rocket experiment. *Adv. Space Res.* **32**, 119.

CRASTER, R. V. & MATAR, O. K. 2000 Surfactant transport on mucus films. *J. Fluid Mech.* **425**, 235.

DAVIS, S. H. 1987 Thermocapillary instabilities. *Annu. Rev. Fluid Mech.* **19**, 403.

DEMEKHIN, E. A., KALLIADASIS, S. & VELARDE, M. G. 2006 Suppressing falling film instabilities by Marangoni forces. *Phys. Fluids* **18**, 042111.

FISHER, L. S. & GOLOVIN, A. A. 2005 Nonlinear stability analysis of a two-layer thin liquid film: dewetting and autophobic behavior. *J. Colloid Interface Sci.* **291**, 515.

HAUT, B. & COLINET, P. 2005 Surface-tension-driven instabilities of a pure liquid layer evaporating into an inert gas. *J. Colloid Interface Sci.* **285**, 296.

HIGGINS, A. M. & JONES, R. A. L. 2000 Anisotropic spinodal dewetting as a route to self-assembly of patterned surfaces. *Nature* **404**, 476.

ISRAELACHVILI, J. N. 1992 *Intermolecular and Surface Forces*. Academic Press.

JOO, S. W. & HSIEH, K.-C. 2000 Interfacial instabilities in thin stratified viscous fluids under microgravity. *Fluid Dyn. Res.* **26**, 203.

LIFSHITZ, E. M. & PITAEVSKII, L. P. 1980 *Statistical Physics*, Part 2. Pergamon.

LIN, Z. Q., KERLE, T., BAKER, S. M., HOAGLAND, D. A., SHAFFER, E., STEINER, U. & RUSSELL, T. P. 2001 Electric field induced instabilities at liquid/liquid interfaces. *J. Chem. Phys.* **114**, 2377.

LIN, Z. Q., KERLE, T., RUSSELL, T. P., SCHAFFER, E. & STEINER, U. 2002a Structure formation at the interface of liquid–liquid bilayer in electric field. *J. Macromolecules* **35**, 3971.

LIN, Z. Q., KERLE, T., RUSSELL, T. P., SCHAFFER, E. & STEINER, U. 2002b Electric field induced dewetting at polymer/polymer interfaces. *J. Macromolecules* **35**, 6255.

MATAR, O. K., CRASTER, R. V. & WARNER, M. R. E. 2002 Surfactant transport on highly viscous surface films. *J. Fluid Mech.* **466**, 85.

MERKT, D., POTOTSKY, A., BESTEHORN, M. & THIELE, U. 2005 Long-wave theory of bounded two-layer films with a free liquid-liquid interface: short- and long-time evolution. *Phys. Fluids* **17**, 064104.

MILADINOVA, S., SLAVCHEV, S., LEBON, G. & LEGROS, J.-C. 2002a Long-wave instabilities of non-uniformly heated falling films. *J. Fluid Mech.* **453**, 153.

MILADINOVA, S., STAYKOVA, D., LEBON, G. & SCHEID, B. 2002b Effect of nonuniform wall heating on the three-dimensional secondary instability of falling films. *Acta Mech.* **156**, 79.

NEPOMNYASHCHY, A. A. & SIMANOVSKII, I. B. 2006 Decomposition of a two-layer thin liquid film flowing under the action of Marangoni stresses. *Phys. Fluids* **18**, 112101.

NEPOMNYASHCHY, A. A. & SIMANOVSKII, I. B. 2007 Marangoni instability in ultrathin two-layer films. *Phys. Fluids* **19**, 122103.

NEPOMNYASHCHY, A. A. & SIMANOVSKII, I. B. 2008 Dynamics of non-isothermic ultra-thin two-layer films. *Microgravity Sci. Technol.* **20** (3–4), 149.

NEPOMNYASHCHY, A. A. & SIMANOVSKII, I. B. 2009a Instabilities and ordered patterns in nonisothermal ultrathin bilayer fluid films. *Phys. Rev. Lett.* **102**, 164501.

NEPOMNYASHCHY, A. A. & SIMANOVSKII, I. B. 2009b Dynamics of ultra-thin two-layer films under the action of inclined temperature gradients. *J. Fluid Mech.* **631**, 165.

NEPOMNYASHCHY, A. A., SIMANOVSKII, I. B. & LEGROS, J. C. 2006 *Interfacial Convection in Multilayer Systems.* Springer.

ORON, A., DAVIS, S. H. & BANKOFF, S. G. 1997 Long-scale evolution of thin liquid films. *Rev. Mod. Phys.* **69**, 931.

POTOTSKY, A., BESTEHORN, M., MERKT, D. & THIELE, U. 2004 Alternative pathways of dewetting for a thin liquid two-layer film. *Phys. Rev.* E **70**, 025201.

POTOTSKY, A., BESTEHORN, M., MERKT, D. & THIELE, U. 2005 Morphology changes in the evolution of liquid two-layer films. *J. Chem. Phys.* **122**, 224711.

POTOTSKY, A., BESTEHORN, M., MERKT, D. & THIELE, U. 2006 Evolution of interface patterns of three-dimensional two-layer liquid films. *Europhys. Lett.* **74**, 665.

SHARMA, A. 2003 Many paths to dewetting of thin films: anatomy and physiology of surface instability. *Eur. Phys. J.* E **12**, 397.

SHARMA, A., KHANNA, R. & REITER, G. 1999 A thin film analog of the corneal mucus layer of the tear film: an enigmatic long range non-classical DLVO interaction in the breakup of thin polymer films. *Colloids Surf.* B **14**, 223.

SHARMA, A. & RUCKENSTEIN, E. 1986 An analytical nonlinear theory of thin film rupture and its application to wetting films. *J. Colloid Interface Sci.* **113**, 456.

SHIKHMURZAEV, Y. D. 2008 *Capillary Flows with Forming Interfaces.* Chapman & Hall/CRC.

SIMANOVSKII, I. B. & NEPOMNYASHCHY, A. A. 1993 *Convective Instabilities in Systems with Interface.* Gordon and Breach.

THIELE, U. 2003 Open questions and promising new fields in dewetting. *Eur. Phys. J.* E **12**, 409.

TREVELYAN, P. M. J., SCHEID, B., RUYER-QUIL, C. & KALLIADASIS, S. 2007 Heated falling films. *J. Fluid Mech.* **592**, 295.

WILLIAMS, M. B. & DAVIS, S. H. 1982 Nonlinear theory of film rupture. *J. Colloid Interface Sci.* **90**, 220.